Characterization of *USH1C*/harmonin in the human retina provides insights into pathophysiology and therapy options for Usher syndrome

Kerstin Nagel-Wolfrum[1,2], Benjamin R. Fadl[1,3], Mirjana M. Becker[1], Kirsten A. Wunderlich[4], Jessica Schäfer[1], Daniel Sturm[1,2], Burcu Gür[1], Lew Kaplan[4], Tobias Goldmann[1], Matthew Brooks[3], Margaret R. Starostik[3*], Anagha Lokhande[3], Melissa Apel[6], Karl R. Fath[1,7], Katarina Stingl[8], Susanne Kohl[9], Miguel Andrade[5], Jan M. Vetter[6], Norbert Pfeiffer[6], Antje Grosche[4], Anand Swaroop[3], Uwe Wolfrum[1#]

[1]Institute of Molecular Physiology, Johannes Gutenberg University Mainz, Germany

[2]Institute of Developmental Biology and Neurobiology, Johannes Gutenberg University Mainz, Germany

[3]Neurobiology, Neurodegeneration and Repair Laboratory, National Eye Institute, National Institutes of Health, Bethesda, USA

[4]Department of Physiological Genomics, BioMedical Center, Ludwig-Maximilian University, Munich, Germany

[5]Computational Biology and Data Mining, Institute of Organismic & Molecular Evolution Biology, Johannes Gutenberg University Mainz, Germany

[6]Department of Ophthalmology, University Medical Centre Mainz, Germany

[7]Queens College of CUNY, Kissena Blvd, Flushing, NY 11367, USA

[8]University Eye Hospital, Centre for Ophthalmology, University of Tübingen, Germany

[9]Institute for Ophthalmic Research, Centre for Ophthalmology, University of Tübingen, Germany

[#]Corresponding author: Uwe Wolfrum, Molecular Cell Biology, Institute of Molecular Physiology, Johannes Gutenberg University Mainz, Hanns-Dieter-Hüsch-Weg 17, Germany; E-mail: wolfrum@uni-mainz.de

*Current addresses:

MRS: Department of Biology, Johns Hopkins University, Baltimore, MD, USA

Abstract

Human Usher syndrome (USH) is a complex genetic disorder that comprises three clinical subtypes USH1, USH2 and USH3 and the most common form of hereditary combined deaf-blindness. Since rodent USH1 models do not reflect the ocular phenotype observed in human patients to date only little is known about the pathophysiology of USH1 in the human eye. The *USH1C* gene is heavily alternatively spliced and encodes for numerous harmonin isoforms that function as scaffold proteins and organizer of the USH interactome. RNA-seq analysis of *USH1C* revealed harmonin a1 as the most abundant transcript of *USH1C* in the human retina. Bulk mRNA-seq and Western blots confirmed abundant expression of harmonin in Müller glia cells (MGCs) and retinal neurons. We located harmonin in the terminal endfeet and apical microvilli of MGCs and in photoreceptor cells (PRCs), particularly in cone synapses and outer segments of rods as well as at adhesive junctions between both, MGCs and PRCs in the outer limiting membrane (OLM). We evidenced the interaction of harmonin with OLM molecules and rhodopsin in PRCs. We correlate the identified harmonin subcellular expression and colocalization with the clinical phenotype observed in USH1C patients. Furthermore, we demonstrate a phenotype in primary cilia in patient-derived fibroblasts which we were able to revert by gene addition of harmonin a1. Our data provide novel insights for retinal cell biology, USH1C pathophysiology and subsequent gene therapy development.

Keywords: Usher syndrome, USH1C, retina dystrophy, harmonin, splicing variants, photoreceptor cells, Müller glia cell

Introduction

The Usher syndrome (USH) is a complex, clinically and genetically heterogeneous disease and leads to the most frequent cause of deaf-blindness in human affecting between one in 6,000 and 10,000 individuals (Friedman et al, 2011; Kimberling et al, 2010). USH is considered a retinal ciliopathy due to the defect in photoreceptor cilia and dysfunction of the primary cilia (Bujakowska et al, 2017; May-Simera et al, 2017; Samanta et al, 2019). Three clinical subtypes of USH (USH1, USH2, USH3) have been described, based on the severity and age of onset of retinal and inner ear impairment (Mathur & Yang, 2015). USH1 is the most severe subtype, characterized by profound congenital hearing impairment or deafness, vestibular dysfunction, and early onset of progressive *Retinitis pigmentosa* (Fuster-Garcia et al, 2021).

Up to now, 10 USH-associated genes and several additional loci have been identified. For USH1, six genes have been identified: *MYO7A* (USH1B), *USH1C*, *CDH23* (USH1D), *PCDH15* (USH1F), *USH1G* and *CIB2* (USH1J). While the assignment of *CIB2* as an USH1 gene has been recently doubted (Booth et al, 2018; Michel et al, 2017; Riazuddin et al, 2012), *ESPN* has been considered as USH1M (Ahmed et al, 2018). Identified USH genes encode proteins from different protein families that collectively function in dynamic networks at different subcellular locations in both the eye and the inner ear. The human *USH1C* gene (ENSG00000006611, OMIM 276904) encodes for the harmonin protein and is located on chromosome 11 (chr 11:17,493,895-17,544,416 on GRCh38.p10). The gene consists of 28 exons exons spread over 50.5 kb of genomic sequence (Figure 1A), and 11 distinct transcripts (splice variants) have been annotated so far in human (Ensembl ENSG00000006611) (Reiners et al, 2006).

Ush1c transcripts in retinae of mice are highly alternatively spliced and encode for a variety of protein isoforms (Zwaenepoel et al, 2001). Analysis of the murine retina revealed at least nine different isoforms encoding for three different classes (a, b and c), classified by the domain content in the expressed harmonin protein (Figure 1; (Reiners et al, 2006; Verpy et al, 2000) (www.ensembl.org). The most characteristic domains of all harmonin isoforms are the ~90-100 amino acid long PDZ domains, named for three scaffold proteins originally recognized to contain these sequences PSD-95, DLG, and ZO-1 (Kim & Sheng, 2004). PDZ domains contain a hydrophobic pocket that associate with PDZ binding motifs (PBM) mostly found at the *C*-terminus of the target protein. Most of the interacting partners of harmonin bind to the up to three PDZ domains in the harmonin isoforms, thus conferring harmonin as a scaffold protein having a central position in the protein interactome related to USH (Kremer et al, 2006; Reiners et al, 2006). Besides myosin VIIa (USH1B), cadherin 23 (USH1D), and SANS (USH1G), the USH2 proteins USH2A and VLGR1 (USH2C) bind to PDZ1, whereas cadherin 23 (USH1D)

and protocadherin 15 (USH1F) bind to PDZ2 in harmonin. Furthermore, SANS can interact with PDZ3. In addition to the PDZ domains, a globular N-domain which increases the binding affinity to proteins binding to PDZ1, such as SANS or VLGR1 and USH2A (Adato et al, 2005; Reiners et al, 2005; Yan et al, 2010) and a CC (coiled-coil) domain are found in all harmonin isoforms. Harmonin b, the longest isoform, is characterized by a second CC domain followed by a PST (proline-serine-threonine rich) domain which facilitates actin filament binding and bundling (Boeda et al, 2002). In addition, harmonin interactions with non-USH proteins have been described for specific cellular compartments, such as the subunits of voltage-gated Ca^{2+}-channels at ribbon synapses (Gregory et al, 2011; Gregory et al, 2013) and the GTPase regulator DOCK4 in stereocilia (Yan et al, 2006), which specify harmonin functions there.

Alternative splicing of *USH1C* transcripts affects the composition of the resulting protein and thereby might influence its cellular function in relevant tissues. USH1C/Harmonin isoforms are expressed in a wide range of tissues, but the results from preliminary studies on the expression and subcellular localization of harmonin in rodent retinae have been contradictory contradictorily (Reiners et al, 2003; Reiners et al, 2005; Sahly et al, 2012; Verpy et al, 2000; Williams et al, 2009). Based on the depicted subcellular localization of harmonin isoforms in rodent photoreceptor cells (PRCs), others and we have suggested differential scaffold functions of harmonin particularly in the outer segment and the synapses (El-Amraoui & Petit, 2005; Millan et al, 2011; Reiners et al, 2003; Reiners et al, 2005; Reiners et al, 2006).

A putative synaptic function was also indicated in the murine retina (Williams et al, 2009) and has been affirmed in zebrafish morpholino knock-downs (Phillips et al, 2011). In the human retina, harmonin has also been found along with other USH proteins in the calyceal processes of cones and rod PRCs (Sahly et al, 2012). It is thought that these extensions of the inner segment of the PRCs stabilize the light-sensitive outer segment of the cell against mechanical forces (May-Simera et al, 2017; Schietroma et al, 2017). Interestingly, the PRCs of most vertebrates possess calyceal processes, except for rodents, and it is currently believed that the lack of calyceal processes in mice is actually responsible for the lack of a retinal phenotype in the numerous mouse models for USH1 including Ush1c, which is comparable to human USH1 patients (Sahly et al, 2012; Schietroma et al, 2017; Williams, 2008).

In previous work, it was assumed in the retina that *USH1C*/harmonin is mainly expressed in PRCs and to a lesser degree in secondary retinal neurons (Reiners et al, 2003; Reiners et al, 2006; Sahly et al, 2012; Williams et al, 2009). However, recently, it became evident that harmonin is also substantially expressed in Müller glia cells (MGCs) (Phillips et al, 2011). More recent studies performed by single cell (sc)RNA-seq of human retinal cells even indicated that

USH1C expression and the expression of some other USH genes is almost restricted to MGCs in human retina (Cowan et al, 2020; Xu et al, 2020). MGCs are the radial glial cells of the retina. They extend from the outer limiting membrane throughout all retinal layers. They terminate with their endfeet at the extracellular inner limiting membrane which separates the neuronal retina from the vitreous. Functionally, they maintain not only the structural integrity of the retina, but are also essential for retinal homeostasis and physiology (Bringmann et al, 2006; Gao et al, 2021). However, nothing is currently known about the subcellular localization of harmonin in the MGCs and how harmonin contributes to their complex functions.

For the development of ocular gene augmentation therapies, it is necessary to understand the expression profile of *USH1C*/harmonin so as to know which *USH1C*/harmonin isoform to introduce and into which retinal cell types (Nagel-Wolfrum et al, 2014). In this study, we deeply investigated the expression of *USH1C*/harmonin on transcript and protein level in the human retina by RNA-seq methods and Western blotting as well as correlative and *in situ* imaging techniques. We demonstrate that *USH1C* is heavily spliced and identify harmonin a1 as the most prominent isoform in the human retina. We confirmed *USH1C*/harmonin expression in MGCs but also detected substantial expression in retinal neurons applying bulk RNA-seq and Western blotting. We show the subcellular localization of harmonin in MGCs and in different compartments of rod and cone PRCs, namely in the outer segments of rods and the synaptic pedicles of cones. In addition, we provide evidence for novel interacting proteins of harmonin in these compartments. Finally, we identify altered cilia length in USH1C patient-derived fibroblasts as an important pathomechansim and are able to revert the pathogenic phenotype by gene addition of harmonin a1 to patient cells.

Results

USH1C is frequently spliced in the human retina.

Our initial goal was to elaborate the transcriptomic profile of USH1C in the human retina, which despite multiple hints is unknown so far. We analyzed the *USH1C*/harmonin splice variants we using complementary methods. The retinal expression of all three classes of *USH1C*/harmonin isoforms was validated by RT-PCR with RNA from five different healthy human donor retinae (Figure 1B-D, Supplemental Table S1). To differentiate between differentially splice isoforms of *USH1C*/harmonin, we designed primer sets specific for all isoforms and each splice variant class, respectively based on human *USH1C* sequences archived in genome databases (http://www.ncbi.nlm.nih.gov/gene/10083). RT-PCR revealed amplicons specific for all three

isoform classes a, b and c (Figure 1B). qRT-PCRs of three human donor retinae demonstrated presence of ~83% *USH1C*/harmonin a and ~2% *USH1C*/harmonin b splice variant (Figure 1C, D). Therefore, remaining isoform classes (c and d, see below) should be present at ~15%.

Next, we analyzed the local splicing events of the *USH1C* gene in the human retina using RNA-seq. We generated an RNA-seq library of the human retina with approximately 90 million reads and 151bp paired-end read-length and analyzed aligned RNA-seq data using Sashimi plots (Figure 1E). We observed alternative splicing of *USH1C* in the human retina, and grouped the alternative splicing events into four regions, namely exons 1 and 5 (region 1), exons 10 and 12 (region 2), exons 14 and 22 (region 3), and exons 25 and 28 (region 4) (Figure 1E). For the quantification of the observed local splice variants (LSV), we utilized additional 50 previously published RNA-seq samples (Pinelli et al, 2016). First, we merged the different samples to receive a total of 10 merged samples with an even read sequencing depth of ~50 million reads. We then quantified each observed LSV with the merged samples. Only LSVs with a minimum of 20 raw counted reads in at least half of the merged samples were used for any downstream analysis.

The LSV ex(1-5) is the most frequent LSV in region 1 of *USH1C* with about 82% read coverage within region 1 (Figure 1F). A novel LSV ex(1,3-5), in which exon 2 is skipped (~9% read coverage), leads to a frameshift and a premature stop codon in exon 3. LSV ex(2-5) is characterized by an alternative start and had an abundance of about 8% among all LSVs in region 1.

In region 2 (exons 10-12), we observed two LSV which differ in the presence or absence of exon 11. Exon 11 was present in about two thirds of the reads. LSV ex(10,12) does not shift the open reading frame (ORF) and can be translated into a *USH1C*/harmonin isoform with a slightly shortened PDZ2 domain. Both LSVs are known and annotated in the transcripts for *USH1C*/harmonin a1 (transcript ID: ENST00000318024) and a4 (transcript ID: ENST00000527020), respectively.

The alternative splicing in region 3 (exons 14-22) was very complex. On the protein level, this region encodes for the CC2 and PST domain, which are only present in *USH1C*/harmonin class b isoforms. The most frequent LSV in region 3 was LSV ex(14,15,22) having about 72% read coverage (Figure 1F). This LSV lacks the CC2 and PST domains and therefore encodes for *USH1C*/harmonin class a or c. LSV ex(14,16-22) was only covered with a very low number of reads in the RNA-seq samples. However, this LSV encodes for the CC2 and PST domains indicating a low but nevertheless existing expression of *USH1C*/harmonin isoform class b in the human retina. Thus, these RNA-seq data confirmed the qRT-PCR results shown in Figure

1B-D. We further found two potentially new exons (16' and 21') located between exon 16 and 17, and 21 and 22, respectively, and a putative alternative 5' splice site of exon 22, all of which have yet to be validated further.

Detailed analysis in region 4 of *USH1C* human retina samples revealed three LSVs. LSV ex(25,26,28) is the most frequent splicing event with a read coverage of about 90%. Two novel exons, exons 25' and 26' which were previously not described for *USH1C* were also observed. (Figure 1F). Exon 25' was part of LSV ex(25,25',26,28) and exon 26' was part of LSV ex(25,26',28), both with a read coverage of about 5% in region 4 of *USH1C*.

To translate our *in-silico* data into peptide sequences we combined the most abundant LSVs of regions 1, 2 and 4 with each LSV found in region 3 and subsequently used these in the online tool SMART (http://SMART.embl-heidelberg.de) to predict the domain structure (Figure 1G). Most LSVs were assigned to the *USH1C*/harmonin classes a, b and c (Reiners et al, 2006; Verpy et al, 2000). In addition, we found a putative novel class for harmonin, which we named *USH1C*/harmonin class d that is similar to harmonin a, but additionally carries a CC2 domain (Figure 1G). ~78% of all LSVs in region 3 were predicted to result in *USH1C*/harmonin a isoforms, of which approximately two thirds are *USH1C*/harmonin a1 and the remaining harmonin a4 depending on the splicing of exon 11 (region 2). This quantification indicated that ~50% of all harmonin expressed in the human retina is *USH1C*/harmonin a1.

USH1C is highly expressed in both Müller glia cells and retinal neurons.

To assign *USH1C* transcripts to specific cell types of the human retina, we performed bulkRNA-seq from sorted MGCs and retinal neurons (RNs) from human retina. As described above, we grouped the splicing events into four regions and set a cut-off of 5% for each LSV per region (Figure 2A). In all four regions *UHS1C*/harmonin transcripts were identified in RNs (and MGCs). In region 1, LSV ex(1-5) was the most frequent LSV, for both RNs and MGCs. Interestingly, expression of LSV ex(1-5) was increased in MGCs compared to RNs. In addition to LSV ex(1,3-5) and LSV ex(2-5), which both were expressed in the two cell types, we identified LSV ex(1,5) in RNs only. In region 2, we observed the two LSVs which have been identified in the RNA-seq of the entire human retina having no significant differences in the number of LSV between RNs and MGCs. In region 3, our bulk RNA-seq revealed 3 LSVs (cut-off 5%). Here, the most frequent transcript was LSV ex(14,15,22), slightly higher expressed in MGCs compared to RNs. LSV ex(14,15,20-22) and LSV ex(14,15,21,22), encoding for the C-terminal part of the PST domain were detected, too. However, in contrast to the RNA-seq of the total retina, no LSV ex(18,19) encoding the entire PST domain was detected, probably due

to lower sequencing depth. In region 4, LSV ex(25,26,28) was the most abundant LSV and expressed in both RNs and MGCs. In summary, our data demonstrate *USH1C* transcripts in both MGCs and RNs. Overall, the relative expression of the different LSVs between RNs and MGCs was quite similar and comparable to the quantification of the whole retinal samples.

Harmonin protein expression and localization in human retinae.

To assess harmonin protein expression in the human retina, we analyzed protein lysates of human donor retinae by Western blots using an harmonin antibody (H3), generated against a conserved *N*-terminal epitope (amino acids 1-89) of harmonin (Reiners et al, 2003), which is suitable for detecting all five isoform groups of harmonin. Western blot analysis demonstrated two major bands at a molecular weight close to 70 kDa (Figure 2B). The reference harmonin_a1 recombinantly expressed in HEK293T cells identified these bands as harmonin a isoforms (Figure 2C), which agrees with our RNA-seq data (Figure 1). In addition, we observed much less prominent higher molecular bands and two prominent lower molecular bands at molecular weights of ~ 45 and ~ 38 kDa. The lower molecular bands most probably represent group c splice variants of harmonin (Reiners et al, 2003; Scanlan et al, 1999), but may also be protein degradation products of higher molecular species. The absence of any harmonin band in the Western blots of the harmonin deficient tissue of a USH1C pig model, that has recently been generated and characterized (Grotz et al, 2021) and siRNA-mediated knock downs of *USH1C*/harmonin in HEK293T cells validated the specificity of our H3 antibody (Figure 2D). Analysis of retinal cell fractions enriched for different cell types of the human retina, revealed harmonin protein variants in fractions of both MGCs and RNs (Figure 2E).

To localize harmonin´s expression in retinae of human and non-human primates we immunostained harmonin in longitudinal retinal cryosections (Figure 2F). Fluorescence microscopy revealed intense harmonin immunofluorescence in the outer segment layer of photoreceptor cells and in the outer limiting membrane (OLM) of human and non-human-primate retinae. In addition, we observed less intense immunostaining in the photoreceptor inner segment, the outer and inner plexiform layers as well as the ganglion cell layer of human and non-human primate retinae.

Co-localization and interaction of harmonin with compounds of the OLM junction complexes between photoreceptor and Müller glia cells

The OLM is characterized by heterotypic cell-cell adhesions between the membranes of photoreceptor and MGCs composed of protein compounds from both adherent and tight

junctions (Omri et al, 2010). Immunofluorescence double-labelling of harmonin and β-catenin, a component of the adherent junctions (Golenhofen & Drenckhahn, 2000) and the tight junction molecule JAM-B (Daniele et al, 2007), respectively showed partial co-localization of harmonin with both junction proteins (Figure 3A). GST-pull downs of the GST-tagged β-catenin and JAM-B from HEK293T cell lysates demonstrated that the interaction of the *C*-terminal tails of both OLM junction proteins with His-tagged harmonin_a1 (Figure 3B, C). Reciprocal interaction pull-downs of GST-tagged PDZ domains revealed the binding of the *C*-terminal tail of β-catenin to the PDZ1 and PDZ3 domain of harmonin (Supplemental Figure S1A). Furthermore, yeast two-hybrid assays demonstrated the interactions of β-catenin and JAM-B with harmonin is direct (data not shown). Likely β-catenin binds to the PDZ1 and PDZ3 domains of harmonin via a *C*-terminal type-I PDZ binding motif (DTDL) (DuChez et al, 2019). In contrast, JAM-B contains a canonical type II PDZ targeting motif (FLV) at position 298-300 of its *C*-terminus, which is probably responsible for binding to harmonin (Ebnet et al, 2003).

The higher resolution of immunoelectron microscopy of ultrathin sections through the OLM of the human retina revealed the localization of harmonin at both sides of the OLM junctions in the photoreceptor cells and MGCs (Figure 3D, E; black arrows). In addition, harmonin was labeled specifically in the tips of microvilli (Figure 3D, E; white arrows) and abundantly in endfeet of the MGCs at the inner limiting membrane (Figure 3F).

Differential expression of harmonin in rod and cone photoreceptor synapses

Next, we determined the localization of harmonin in the photoreceptor synapses of the outer plexiform layer. Because the synaptic regions of the human donor retinae were not well preserved, perhaps due to postmortem degradations, we expanded our analyses to non-human primate (NHP) retinae (see also Figure 2B). Immunofluorescence double staining revealed partial overlap of harmonin and the characteristic horseshoe-like staining of RIBEYE, a marker of the synaptic ribbon of (tom Dieck & Brandstatter, 2006) in photoreceptor synapses in both human and non-human primate sections (Figure 4A). Immunoelectron microscopy of NHP retinae allowed us to confirm the localization of harmonin at the photoreceptor synapses (Figure 4B). Interestingly, TEM analyses revealed dense harmonin labelling in pedicles of cones while the labelling in rod spherules was much weaker (Figure 4B, C).

Previous studies have indicated that harmonin interacts with voltage-gated L-type Ca^{2+}-channels at ribbon synapses of inner ear hair cells and retinal photoreceptor cells (Gregory et al, 2011; Gregory et al, 2013; Kersten et al, 2010) The Ca^{2+}-channels are bridged by filamin-A to the actin cytoskeleton (Lodha et al, 2010). GST-pull downs of the GST-tagged filamin-A, an

actin binding protein, from HEK293T cell lysates demonstrated the interaction of the *C*-terminal tails filamin-A with His-tagged harmonin_a1 (Figure 4D). Immunofluorescence analysis of retinal sections revealed that harmonin and filamin-A are co-distributed in the outer plexiform layer (Figure 4E). Taken together these data suggest that filamin-A is a novel interaction partner of harmonin at ribbon synapses.

Differential expression of harmonin in the outer segments of rod and cone PRCs cells

Immunofluorescence microscopy showed the presence of harmonin in the outer segment layer of the human retina (Figures. 2F, 5A). To discriminate between rod and cone outer segments, we stained longitudinal cryosections through the human retina with anti-harmonin and FITC-conjugated peanut agglutinin (PNA), a common marker for cones (Blanks & Johnson, 1984). Confocal analyses did not demonstrate a co-localization of harmonin and PNA in longitudinal sections (Figure 5B). This was confirmed by maximum projections of confocal planes of fluorescence images and z-sections of maximum projections. Furthermore, the overlay of fluorescent intensity plots of anti-harmonin and FITC-PNA staining revealed apparent dissimilarities in their peaks (Figure 5C; low Pearson correlation coefficient values: Rr:0.18; M1:0.18; M2:0.19). In contrast, fluorescent intensity plots of harmonin and rod specific arrestin-1 immunofluorescence staining showed apparent signal convergences (Figure 6C; high Pearson correlation coefficient values: Rr:0.59; M1:0.57; M2:0.42) suggesting harmonin expression in rod, but not in cone outer segments.

Immunoelectron microscopy of human photoreceptor cells confirmed our confocal data: harmonin labelling was found in the outer segments of rods but not of cones (Figure 5E-G). In the rod outer segments, harmonin immunostaining was found at the bases where outer segment discs are formed *de novo* and throughout the outer segment along the cytoplasmic side of the disc membranes (Figure 5G). In addition, we found harmonin labelling in the calyceal processes of photoreceptor cells as previously described by Sahly et al. (Sahly et al, 2012) (Figure 5E, asterisk). Western blot analyses of purified outer segment fractions of porcine retinae further confirmed the expression of harmonin in photoreceptor outer segments (Figure 6A). Thus, our results suggest that harmonin is associated specifically with the disc membranes of the rod outer segments.

Harmonin interacts with rhodopsin in the human retina

In the microvilli of the rhabdomes of *Drosophila* photoreceptors, functionally homologous to the outer segment discs of vertebrate PRCs, rhodopsin binds to the PDZ domain-containing

scaffold protein INAD (Montell, 1999; Xu et al, 1998). To test whether the PDZ-protein harmonin also interacts with human rhodopsin, we performed *in vitro* co-immunoprecipitation assays with protein lysates from HEK293T cells expressing GFP-rhodopsin and HA-tagged harmonin or RFP-harmonin, respectively. Western blots of the recovered proteins revealed that harmonin a1 co-precipitated with GFP-rhodopsin, but not in controls with GFP alone (Figure 6B; Supplemental Figure S1B).

To examine a putative interaction of harmonin and rhodopsin in the human retina, we performed *in situ* proximity ligation assays (PLA) applying anti-harmonin (H3) and monoclonal antibodies to rhodopsin in unfixed retinal cryosections (Figure 6C). We observed positive PLA signals in the photoreceptor layer, predominately in the outer segment layer and a significant smaller numbers of signals in the inner segment (Figure 6C,D). In contrast, almost no positive PLA signals were found in the controls (Figure 6C).

In summary, harmonin localization in rod outer segments shown by complementary light and electron microscopic methods, paired with the interaction of harmonin and rhodopsin *in vitro* and the close proximity of both proteins in the photoreceptor layer demonstrated by *in situ* PLAs suggests that rhodopsin and harmonin interact in the outer segment of rods.

Retinal phenotype and ciliary phenotype in fibroblast of USH1C patients

Two male siblings with confirmed mutations in *USH1C* (c.91C>T;p.(R31*), c.238dupC;p.(Arg80Profs*69)) were clinically examined at the age of 35 and 47 years, respectively. Their clinical findings are shown in Figures 7A-E and Supplemental Figure S2, respectively. Optical coherence tomography (OCT) of the 35-years old male patient revealed atrophy and thinning of the outer/inner segment PRCs layer and the outer nuclear layer up to the fovea, typical for PRCs loss in RP. The outer retina atrophy corresponded to a progressed constriction of the visual field borders on around 5 degrees and a hyperfluorescenr perifoveal ring on the fundus autofluorescence imaging (Fig 7B). Additionally, in OCT, epiretinal gliosis was observed, that is a common complication of RP and which we recently found as a hallmark in the retina of the USH1C pig model generated by introducing the human exon 2 bearing the c.91C>T;p.(R31*) nonsense mutation into the porcine *USH1C* gene (Grotz et al, 2021). The posterior eye pole showed typical bone spicula in the mid periphery and periphery (Fig. 7A). Still, with a progressed peripheral retinal degeneration at 35 years, the central vision was relatively well preserved with visual acuity of 20/25 on both eyes and normal colour perception (Figure 7E).

The outer segment of photoreceptor cells resembles a highly modified primary sensory cilium (Bujakowska et al, 2017; May-Simera et al, 2017). We analysed the primary cilia on dermal fibroblasts derived from an USH1C$^{R80Pfs*69/R31*}$ patient after induction of ciliogenesis (Samanta et al, 2019). The primary cilia of USH1C patient fibroblast were significantly longer when compared the primary cilia of healthy donor fibroblasts (Figure 7F-I). Strikingly, this ciliary phenotype of USH1C $^{R80Pfs*69/R31*}$ patient fibroblast was rescued by the re-expression of harmonin_a1 (Figure 7F,I). These data suggest that fibroblasts from USH1C patients could be a potential cellular model for evaluating therapies for USH1C and that the harmonin a1 isoform is able to reverse the patient´s cellular phenotype to the normal one.

Discussion

Our results show that *USH1C* is heavily alternatively spliced in the human retina. We do not expect that all variants will be translated into protein due to pre-translational processing of mRNAs (Vogel & Marcotte, 2012).

. Nevertheless, we assume that several *USH1C*/harmonin isoforms are expressed, potentially with distinct patterns in the various human retinal cell types. Harmonin is a scaffold protein that is modularly composed of well-defined domains and motifs, such as PDZs, CCs and a PBM (Fig. 1A,G),which are suitable for protein-protein interaction (Reiners et al, 2006). The binding affinity of interacting proteins can be enhanced by the harmonin *N*-domain (Yan et al, 2010). Assignment of the identified LSVs in the human retina to these domains revealed that alternative splicing may affect binding of target molecules to harmonin in human retinal cells. For example, alternative splicing of exon 2 in region 1 should alter the globular *N*-domain and affect the binding affinity of harmonin PDZ1 to target proteins, such as VLGR1 (USH2C), USH2A and SANS (USH1G) (Adato et al, 2005; Reiners et al, 2005). This is in line with our recent results indicating a reduced binding affinity of target proteins to harmonin lacking parts of the *N*-domain (Sturm, 2020 Master Thesis). Furthermore, splicing out of exons 16-21 in region 3 leads to loss of the CC2 and PST domains, which should reduce oligomerization of harmonin molecules and the loss of actin filament bundling properties, respectively (Boeda et al, 2002).

The differential binding of proteins to the harmonin splice variants may also imply differences in the functions of harmonin in cells of the retina. Accordingly, the control and

regulation of alternative splicing of USH1C/harmonin in the retina is of importance. Previous studies have identified Musashi proteins (MSI1 and MSI2) as important regulators of alternative splicing in the retina (Ling et al, 2020; Murphy et al, 2016; Sundar et al, 2021). However, USH1C/Harmonin has not been identified as a target for the splicing control machinery of Musashi proteins. Recently, we were able to show that the USHG1 protein SANS interacts with core components of the spliceosome and regulates splicing including constitutive and alternative splicing of USH1C/harmonin (Yildirim et al, 2021). In particular, the latter study show that SANS causes the retention of exon 11 and thus the alternative expression of the human harmonin a1 and a4 transcripts. Future studies are important and necessary to understand the interplay and interference of the two USH1 proteins SANS and harmonin in the retina at two different levels: in common protein complexes (SANS-SAM/PBM binding to the N-domain and PDZ3 of harmonin), possibly related to transport processes (Adato et al, 2005; Maerker et al, 2008; Yan et al, 2010), and during splicing, where SANS presumably can interfere with USH1C/harmonin pre-mRNA (Yildirim et al, 2021).

The assignment of LSVs to the harmonin domains also allowed us to quantify the expression of the harmonin classes in the human retina (Figure 1G). This analysis demonstrates that harmonin a is by far the most abundant class expressed in the human retina which agrees with our results obtained by semi- and quantitative RT-PCR of human donor retinae (Figure 1B-C) and the protein size (~ 70 kDa) detected by Western blots (Figures 2B-E). Our data also indicate that in the human retina harmonin a class the harmonin a1 transcript is more frequently expressed compared to the harmonin a4 (exclusion of exon 11) isoform. From this we propose that harmonin a1 is the most promising variant for gene replacement therapies which is strengthened by the rescue of the pathogenic phenotype in primary cilia in fibroblasts of USH1C patient after addition of harmonin a1 (Figure 7).

The human retina consists of seven distinct neural cell types, five types of RNs and two types of glia cells, mainly MGCs and microglia cells (Rodieck 1998, First Steps in seeing). In contrast to a common hypothesis in the field that USH1 molecules are mostly expressed in PRCs (Reiners et al, 2003; Sahly et al, 2012), our results reveal *USH1C*/harmonin expression in both RNs (which include mainly PRCs) and MGCs in the human retina. We found almost equal levels of *USH1C* expression in RNs and MGCs (Figure 2A) by bulkRNA-seq of retinal cells purified from human donor retinae. Of note, we did not observe substantial differences in LSV expression levels in RNs and MGCs. These observations contrasts data from a recently published scRNA-seq study of human retinal cells, which reported that USH1C expression is almost exclusively restricted to MGCs in the human retina (Cowan et al, 2020). The discrepancy

between our bulkRNA-seq results and the latter data sets obtained by scRNA-seq might be due to differences in the sequencing depth of the two different techniques applied. In addition, scRNA-seq requires tissue dissociation prior to library preparation, which is a crucial step and small imbalances in tissue dissociation, especially in retinal cells, can have a huge impact on the gene expression profile (Fadl et al, 2020). Nevertheless, our results from bulkRNA-seq are consistent with our results from harmonin protein expression in the human retina. Results from both Western blot analyses of the retinal fractions of RNs and MGCs and from present immunocytochemical studies by light and electron microscopy revealing expression and subcellular localization of harmonin in MGCs and PRCs are consistent with our bulkRNA-seq results (Figures 2-5).

Recent studies and our present study consistently show that USH1C/harmonin is expressed in MGCs of the human retina (Cowan et al, 2020; Phillips et al, 2011). Here, we show the localization of harmonin in distinct subcellular compartments of human MGCs which may provide first hints for harmonin function in MGCs. Immunoelectron microscopy revealed the localization of harmonin at the tips of the microvillar processes formed by their apical membrane of MGCs which project into the subretinal space surrounding the PRC inner segments (Figure 3D and E). This distinct localization is not only consistent with the presence of harmonin in the tip-link complex of stereocilia (which resemble modified microvilli of auditory hair cells (Grillet et al, 2009; Wu et al, 2012), but also with the localization of harmonin in the very similar tip-link complex of the brush border microvilli of intestinal enterocytes (Li et al, 2016). In contrast to tip-link complex of stereocilia where harmonin interacts with all other USH proteins, in the brush border microvilli tip-link, harmonin forms together with ANKS4B and MYO7B a stable ternary complex for anchoring microvilli tip-link cadherins such as CDHR2 and CDHR5 (Crawley et al, 2014; Li et al, 2016). Other than the localization of harmonin, to date nothing is known about the further molecular composition of the putative tip-link complex of MGCs microvilli. However, a morphologic similarity between the microvilli of MGCs and the brush border microvilli is evident. The absence of tip-link molecules in brush border microvilli leads to structural perturbations linked to ineffective epithelial transport (Pinette et al, 2019). An effective transmembrane transport is also essential for the function of MGCs (Bringmann et al, 2006) and harmonin may contribute to the structural arrangement and the physiological function of the microvilli populated apical MGC membrane.

We also found abundant harmonin expression in conical endfeet at the other pole of the MGCs adjacent to the inner limiting membrane and vitreous humor (Figure 3F). There,

harmonin may be integrated into protein networks which mechanical stabilizes the endfeet at the MGC basis and supports anchoring MGCs at the inner limiting membrane.

In addition, we show a prominent submembranous localization of harmonin in MGCs and PRCs associated with the specialized heterotypic adhesion junctions of the OLM (Figure 3A,D,E). Partial co-localization of harmonin and β-catenin, a linker of cadherins to actin filaments, and the transmembrane protein JAM-B, together with the binding of the cytoplasmic tails of both proteins to harmonin strongly suggest that harmonin provide the molecular scaffold to anchor both proteins in the submembranous cytoplasm perhaps to the actin cytoskeleton at the OLM junctions. Defects in the heterotypic adhesion junction complexes of the OLM can disturb the structural integrity of the retina (adhesion part) and/or increase the permeability (tight junctional part) of the retinal barrier (Omri et al, 2010). Since harmonin interacts with both parts, its deficiency may affect both adhesion and barrier function of the OLM. In pathological conditions in patients the disruption of the retinal barrier function of the OLM contributes to fluid accumulation in the macula that can clinically manifest as a macular edema. Although macular lesions are also found in other hereditary retinal degenerative diseases, macular abnormalities are observed more often in USH patients (Testa et al, 2017). This is also consistent with our observation in clinical inspections of two USH1C patient (Figure 7A-E, Supplementary Figure S2). OCT of both USH1C patients do not only show thinning of PRC layer as expected but also revealed alterations macula. It will be interesting for the future to determine whether these lesions are caused by disturbed leaky OLM adhesion junctions or by other processes *e.g.*, MGC gliosis and inflammation which may provide novel therapeutic options.

As discussed above USH1C/harmonin is also expressed in RNs. In RNs we predominantly found harmonin localization in PRCs in the human and NHP retinae which is consistent with previously data (Sahly et al, 2012). As in MGCs, we also observed the localization of harmonin in diverse subcellular compartments of cone and rod PRCs, namely in submembranous cytoplasm of the basal inner segment at the heterotypic OLM junctions (see above), outer segments, calyceal processes, and ribbon synapses. Previous studies indicate a multifaceted presynaptic role of harmonin in ribbon synapses regulating L-type Ca^{2+} channels and neurotransmitter exocytosis in inner ear hair cells (Gregory et al, 2011; Gregory et al, 2013; Kersten et al, 2010). Here, we show that harmonin coloclizes and interacts with filamin-A, an actin binding protein, that binds to presynaptic Ca^{2+} channels (Lodha et al, 2012) and facilitates surface membrane localization of channels (Rafizadeh et al, 2014). Although we identified harmonin in the ribbon synapses of both PRC types, our immunoelectron microscopy data show

that harmonin is much more abundant in the synaptic pedicles of cones than in rod synaptic terminals. This is consistent with the previously reported role of harmonin in synaptic maturation in cone pedicles in zebrafish (Phillips et al, 2011) and with our recent findings in our USH1C knock in pig model indicating that the harmonin deficiency alters the width of cone synaptic pedicles (Grotz et al, 2021). It is of note that there is evidence from earlier studies for a selective modulation of pre-synaptic L-type calcium currents in cones to broaden the dynamic range of synaptic transfer by controlling the amount of transmitter release from cones (Hosoi et al, 2005) and all in all our data supports a putative role of harmonin contributing to this phenomenon.

The localization of harmonin in the calyceal processes of PRCs is consistent with previous reports (Sahly et al, 2012). There is evidence that cadherin 23 (USH1D) and protocadherin 15 (USH1F) link the membrane of the calyceal processes to the plasma membrane of the outer segment via their long extra cellular domains (Schietroma et al, 2017). In this scenario, harmonin is thought to anchor the USH1 cadherins in the cytoplasm of the calyceal processes mediated by binding of their *C*-terminal PBMs to harmonin PDZ2 which should also provide a link to the actin filament bundles in the calyceal process core.

More strikingly, we consistently found abundant harmonin localization in the outer segment of rod PRCs, whereas no harmonin is present in cone outer segment (Figure 5). There are obvious differences in disc neogenesis and outer segment disc stacking between rod and cone PRCs. In contrast to cones, rod coin-roll like stacked disc membranes become enclosed by the plasma membrane in the course of disc neogenesis at the base of the outer segment (Burgoyne et al, 2015; Goldberg et al, 2016). The localization of harmonin at the base of the outer segment and its ability to bind actin are consistent with an involvement in disc neogenesis processes there, in which the actin cytoskeleton plays a key role (Corral-Serrano et al, 2020; Spencer et al, 2020).

In addition, harmonin lines up along the disc membranes of the entire rod outer segment and may also directly participate in the disc stacking. There is evidence for a network of cytoplasmic membrane-membrane tethers or spacers localized between the outer segment discs, but their molecular identity remains to be rigorously demonstrated reviewed in (Goldberg et al, 2016). Interestingly, harmonin fulfills possible criteria of such spacers: as a scaffold protein, harmonin facilitates protein networks, forms homomers, binds to membranes, directly to phospholipids (Bahloul et al, 2010) or by interacting with transmembrane proteins such as the large disc membrane protein rhodopsin, shown herein (Figure 6B,C; Supplemental Figure S1B). Such roles of harmonin in disc morphogenesis and stacking are in line with our recent

findings on the disturbed disc architecture of rod outer segments in the USH1C pig model, revealing vertically orientated membrane discs, disk stacks infringed by interstitial gaps and vesicle-like structures present at the outer segment base rod (Grotz et al, 2021). Nevertheless, further studies are necessary to test and validate our hypotheses related to harmonin functions in the rod outer segment.

In conclusion, we show that the scaffold protein harmonin is expressed in the human retina in form of numerous splice variants predominantly in PRCs where these localize in diverse subcellular compartments of PRCs and in MGCs. Defects in *USH1C*/harmonin should impair the various functions of PRCs and MGCs in these very distinct subcellular compartments. We hypothesize that these cellular dysfunctions have a cumulative effect, leading to the slow retinal degeneration and visual loss characteristic of USH1C patients. Understanding how these cellular defects interfere, potentially amplify and accumulate will provide new clues to cellular pathophysiology, elucidating potential targets for treatment and cure of USH1C patients. Although we cannot provide a fully elaborated therapeutic concept, we provide evidence that harmonin a1 is the most promising splice variant for gene supplementation therapy and also identify both PRCs and MGCs as the targets for such a therapy of USH1C patients.

Material & Methods

Human Subjects. Procedures adhered to the Declaration of Helsinki and were approved by the institutional review boards. Written informed consent was obtained from patients and probands. All cellular and molecular analyses of human retina was performed using *post-mortem* anonymized samples (Supplemental Table S1). The donors had no history of retinal disease and were either obtained from the Department of Ophthalmology (University Medical Center Mainz, Germany) or from the National Disease Research Interchange (NDRI, Philadelphia, USA). Donors were between 44 and 68 years old. Both genders were present.

Clinical examination. Two sibling patients genetically diagnosed for USH1 with biallelic *USH1C* mutations were examined clinically at the Center for Ophthalmology, University of Tübingen, including high-resolution retinal imaging and multimodal functional diagnostics. The clinical examination included a detailed medical history, best corrected visual acuity (BCVA) testing, color perception evaluation using the Lanthony test, kinetic perimetry (Octopus 900; Haag-Streit International, Wedel, Germany), slit-lamp examination, fundus examination in mydriasis with color fundus photography and 30 degrees fundus

autofluorescence, as well as spectral domain optical coherence tomography (OCT) (Heidelberg Engineering GmbH, Heidelberg, Germany).

Non-human primates (NHP). Eyes from three adult unaffected macaques (Macaque mulatta) were obtained from the German Primate Center (DPZ) where they were sacrificed as controls in other unrelated experiments.

Transcriptome analysis. RNA isolated from 3 retinae of three donors (Table S1) were processed for RNA-seq anlalysis. RNA isolation was performed with "RNeasy Mini Kit" (Qiagen, Hilden, Germany), according to company's instruction. The eluate was used twice to increase the RNA yield. Libraries were generated with Illumina's TruSeq Stranded mRNA Library Prep Kit and sequenced using Illumina HiSeq2500 sequencing platform as stranded, paired-end with a length of 151-nucleotides (mRNA datasets) (*IMSB,* Mainz, Germany). Using the "best practice" pipeline from NEI commons using Trimmomatic (Bolger et al, 2014), STAR (Dobin et al, 2013), and Kallisto (Bray et al, 2016) (https://neicommons.nei.nih.gov/#/howDataAnalyzed), we aligned our sample to the Ensembl transcriptome version 89. The Pinelli samples were downloaded as BAM-files from EBI's ArrayExpress (E-MTAB-4377), reverted to FASTQ-files using SAMTOOLS (Li et al, 2009) and processed the same way as mentioned above. For visualization we used the Integrative Genomic Viewer (IGV, https://www.broadinstitute.org/igv/) (Robinson et al, 2011; Thorvaldsdottir et al, 2013).

Reverse transcription, polymerase chain reactions, subcloning, and identification of LSVs. The RNA isolation was performed using "TRIzol" (Invitrogen in Waltham, USA) according to company's instruction. The reverse transcription (RT-PCR) was performed with "Superscript II Reverse Transcriptase" (Invitrogen in Waltham, USA), according to company's instruction using oligo-T-primer and 7 µl of isolated RNA eluate. The polymerase chain reaction (PCR) was performed with "Taq DNA Polymerase with Standard Taq Buffer" (NEB in Ipswich, MA, USA) according to company's instructions for 25 µl total volume and 40 cycles. Corresponding author will provide primer sequences used on request.

MACS-sorting of human MGCs and RNs. Retinal cell types were enriched as described previously using magnetic-activated cell sorting (MACS) (Grosche et al, 2016). Briefly, retinal punches (6 mm in diameter, centered over the macula and for comparison, the peripheral punch was performed at 1 mm from the macular punch and inferiorly in relation to it) were treated with papain (0.2 mg/ml; Roche Molecular Biochemicals) for 30 minutes at 37°C in the dark in Ca^{2+}- and Mg^{2+}-free extracellular solution (140 mM NaCl, 3 mM KCl, 10 mM HEPES, 11 mM glucose, pH 7.4). After several washes and 4 minutes of incubation with DNase I (200 U/ml), retinae were triturated in extracellular solution (now with 1 mM $MgCl_2$ and 2 mM $CaCl_2$). To

deplete microglial and vascular cells, the retinal cell suspension was subsequently incubated with anti-mouse/human CD11B and anti-human CD31 microbeads according to the manufacturer's protocol (Miltenyi Biotec, Bergisch Gladbach, Germany). The respective binding cells were depleted from the retinal suspension using large cell (LS)-columns, prior to MGC enrichment. To purify MGCs, the cell suspension was incubated in extracellular solution containing biotinylated anti-human CD29 (0.1 mg/ml, Miltenyi Biotec) for 15 minutes at 4°C. Cells were washed in an extracellular solution, spun down, resuspended in the presence of anti-biotin ultra-pure MicroBeads (1:5; Miltenyi Biotec,) and incubated for 10 minutes at 4°C. After washing, CD29+ Müller cells were separated using LS columns according to the manufacturer's instructions (Miltenyi Biotec). Cells in the flow through of the last sorting step - depleted of microglia, vascular cells and MGCs - were considered as the neuronal population.

Bulk RNA-sequencing on purified retinal cell populations. Total RNA was isolated from cell pellets after immunoseparation using the PureLink® RNA Micro Scale Kit (Thermo Fisher Scientific, Schwerte, Germany). RNA integrity validation and quantification was performed using the Agilent RNA 6000 Pico chip analysis according to the manufacturer's instructions (Agilent Technologies, Waldbronn, Germany). Enrichment of mRNA and library preparation (Nextera XT, Clontech), library quantification (KAPA Library Quantification Kit Illumina, Kapa Biosystems, Inc., Woburn, MA, USA) as well as sequencing on an Illumina platform (NextSeq 500 High Output Kit v2; 150 cycles) were performed at the service facility of the KFB Center of Excellence for Fluorescent Bioanalytics (Regensburg, Germany; www.kfb-regensburg.de). After de-multiplexing, at least 20 million reads per sample were detected. Quality control (QC) of the reads and quantification of transcript abundance was performed applying STAR (Dobin et al, 2013). To this end, *cutadapt* was used to remove adapter sequences and several QC measures were queried with *fastqc*. Next, the trimmed reads were aligned to the reference genome/transcriptome (*mm10*) applying STAR and transcript abundance was estimated with RSEM (Li & Dewey, 2011) expressed as **T**ranscripts **P**er kilobase **M**illion (TPM).

Western blot analyses. ¼ of human retinae were placed in 125 µl HGNT-buffer and sonified 3 times á 5 s. For denaturing gel electrophoresis, the samples were mixed with SDS-PAGE sample buffer (62.5 mM Tris-HCL, pH 6.8; 10% glycerol, 2% SDS, 5% mercaptoethanol, 1 mM EDTA and 0.025% bromphenol blue). As a molecular marker PageRuler™ Prestained Protein Ladder ranging from 11 to 170 kDa was used (Fermentas, St. Leon-Rot, Germany). 30 µg retina protein extracts were separated on 8% polyacrylamide gels and blotted onto PVDF transfer membranes (Millipore, Bedford, MA). Blocking with non-fat dried milk (Applichem,

Darmstadt, Germany). Immunoreactivities were detected on Western blot analysis, with primary antibody against harmonin (H3) and appropriate secondary antibody. Detection was performed either by a chemiluminescence detection system or using the Odyssey infra-red imaging system (LI-COR Biosciences, Lincoln, NE, USA. Cell pellets of enriched cell populations from retinal punches (6 mm in diameter) were dissolved in reducing Laemmli sample buffer, denatured and sonicated. Samples were separated on a 12% SDS-PAGE. The immunoblot was performed as previously described (Schafer et al, 2017). Detection was performed with primary and secondary antibodies diluted in blocking solution. Blots were developed with WesternSure PREMIUM Chemiluminescent Substrate (LI-COR, Bad Homburg, Germany). To validate specificity of the antibodies, all of them were tested on human serum and purified proteins as positive control and human serum depleted for the respective complement factor as negative control.

Antibodies and fluorescent dyes. Primary Antibodies used were anti-JAM-B (SAB2501282, Sigma Aldrich), anti-β-catenin, anti-filamin-A and anti-arrestin SCT128 (Santa Cruz Biotechnology, USA), anti-his (GE Healthcare, Amersham^{TM}, Freiburg, Germany), anti-GFP (gift from Eric Pierce) and anti-RFP **(**Chromotek, Planegg-Martinsried, Germany). The antibody against harmonin (H3) was previously described (Reiners et al, 2003). Monoclonal antibodies (mAbs) against bovine rod opsin B6-30a1, K16-155, and R2-15 were applied as previously described (Adamus et al, 1991; Wolfrum & Schmitt, 2000). Subcellular markers were RIBEYE (BD Bioscience, California, USA), the fluorescein labelled lectin peanut agglutinin (FITC-PNA) and 4',6-diamidino-2-phenylindole (DAPI; Sigma Aldrich). Secondary antibodies for immunofluorescence and Western blot analysis were conjugated to Alexa 568 and Alexa 488 (Molecular Probes, Leiden, Netherlands). Detection of anti-harmonin H3 on Western blot via a donkey anti-rabbit secondary antibody coupled to horseradish peroxidase (ECL Plus Western Blotting Detection System, GE Healthcare).

Immunofluorescence microscopy. Non-human primate retinae were directly cryofixed after dissection. Human retinae were cryofixed 11 1/2 to 31 h *post mortem* in melting isopentane and cryosectioned as previously described (Wolfrum, 1991). Cryosections were placed on poly-L-lysine-precoated coverslips and incubated with 0.01% Tween 20 in PBS. PBS washed sections were blocked with blocking solution (0.5% cold water fish gelatine, 0.1% ovalbumin in PBS) for 30 min, and then incubated with primary antibodies in blocking solution overnight at 4°C. Washed sections were subsequently incubated with secondary antibodies and fluorescent dyes in blocking solution for 1-2 h at room temperature in the dark. After washing with PBS, sections were mounted in Mowiol 4.88 (Hoechst, Frankfurt, Germany). Light microscopy analyses of

immunofluorescence were performed with a Leica SP5 confocal laser scanning microscope (Leica microsystems, Bensheim, Germany). Images were processed with Adobe Photoshop CS (Adobe Systems, San Jose, USA). Colocalization analysis were performed with the ImageJ (http://rsbweb.nih.gov/ij/) plugin JACoP (http://rsbweb.nih.gov/ij/plugins/track/jacop.html).

Transmission electron microscopy. Human donor retina samples 199-09 and 121-10 were processed for pre-embedding immunolabelling as previously described (Sedmak et al, 2009). In brief, perforated human eyes were pre-fixed in buffered fresh 4% paraformaldehyde, dissected, infiltrated with buffered sucrose (30%) and cracked by freezing-thawing cycles. After embedding in 2% Agar (Sigma-Aldrich), agar blocks were sectioned with a vibratome (LeicaVT1000 S). Sections were incubated with H_2O_2, carefully washed and subsequently incubated with harmonin H3 antibody for 4 days, followed by overnight with anti-rabbit biotinylated secondary antibody. Reactions were visualized applying a Vectastain ABC-Kit (Vector Laboratories). Stained retina sections were post-fixated first in buffered 2.5% glutaraldehyde and in buffered 0.5% OsO4. Washed and dehydrated specimens were flatmounted between ACLAR® films (Ted Pella Inc., Redding, USA) in Renlam® M-1 resin. Polymerized flatmount specimens were clued on top of empty Araldit blocks. Ultrathin sections prepared with an Ultracut S ultramicrotome (Leica) were collected on Formvar-coated copper. Counter stained ultrathin sections were analyzed with a FEI Tecnai 12 electron microscope. Images were obtained with a charge-coupled device camera (SIS Megaview3; Surface Imaging Systems) acquired by AnalSIS (Soft Imaging System) and processed with Photoshop CS (Adobe Systems).

HEK293T cell culture. HEK293T cells were cultured in Dulbecco´s modified Eagle´s medium supplemented with 10% heat-inactivated fetal calf serum (Invitrogen) and 1% penicillin/streptomycin (Invitrogen) at 37°C and 5% CO_2. Transfections of plasmids were performed with Lipofectamine® LTX and Plus Reagent (Invitrogen, Germany) and siRNAs were transfected using Lipofectamin RNAiMAX, according the manufactures´ protocols, respectively.

Human primary fibroblast cultures. Dermal primary fibroblast lines were expanded from skin biopsies of human subjects. Primary fibroblast lines were cultured in DMEM medium containing 10% FCS and 1% penicillin-streptomycin at 37°C and 5% CO_2.

siRNA knock-down siRNAs against human USH1C/harmonin (siHarm1 and siHarm2) and non-targeting control siRNA (NTC) were purchased by IDT ((TriFECTa® Kit DsiRNA Duplex, IDT, Germany), For knock-downs, HEK293T cells were transfected with harmonin a1-HA (pBI-CMV4-harm_a1-HA), and 20 nM non-targeted control. 24 h later, cells were lysed in

Triton X-100 lysis buffer, protein concertation were determined using BCA assay. Equal amount of protein lysates were subjected to SDS-PAGE, followed by Western blotting. Actin was used as loading control. For quantification, the optical densities of harmonin a1 (~ 80 kDa) bands were ascertained and normalized to the appropriate loading control. The percentage (%) of harmonin a1 expression is shown in relation to harmonin a1-HA transfected cells.

GST pull downs. Constructs encoding harmonin domains were cloned in the vector pDEST17 (Gateway cloning system, Invitrogen, USA) as previously described. The cDNAs encoding *C*-terminal tails of Mm JAM-B tail (amino acids 257-299) (Mm JAM-B (AA690843 /IMAGE: 1195543), Mm β-catenin tail (amino acids 734-782) and filamin A tail (amino acids 2264-2648) were cloned in the vectors pDEST17 and pDEST15 and bacterial expressed. GST-pull down assay were performed as previously described by mixing equal amounts of GST or GST-fusion proteins were mixed with lysates of His-tagged fusion proteins (Reiners et al, 2005).

GFP-Trap®. HEK293T cells were transfected with harmonin a1-HA (pBI-CMV4-harm_a1-HA), GFP-Rhodopsin (pMT3-Rhodopsin-GFP) or GFP (pMT3-Rhodopsin-GFP), respectively, and lysed in TritonX-100 lysis buffer. Protein lysates of transfected cells were precleared using agarose beads. Equal amounts of precleared lysates were diluted in dilution buffer (10 mM Tris/Cl pH 7.5, 150 mM NaCl, 0.5 mM EDTA). 10% of the diluted amount was used as input. GFP-fused polypeptides were immobilized at Trap® agarose beads (ChromoTek) and used for co-precipitation assays according to the manufacturer´s protocol. Briefly, Rhodopsin-GFP and GFP-only lysates were incubated with blocked GFP-Trap® agarose beads (BSA 3% for 2 hours at 4°C, washed with wash buffer (10 mM Tris/Cl pH 7.5, 500 mM NaCl, 0.5 mM EDTA)) for 30 min at 4°C, rotating. After washing, harmonin a1-HA protein lysate was added onto the beads and incubated for 2 h at 4°C. After washing, precipitated protein complexes were eluted with SDS-sample buffer at 65°C. Protein complexes were then subjected to SDS-PAGE and Western blot.

Proximity ligation assay (PLA). For *in situ* proximity ligation assay the Duolink PLA probes anti-rabbit^{PLUS} and anti-mouse^{MINUS}, and the Detection Reagent Red were purchased from Sigma (Weibrecht et al, 2010) was performed on HEK293T cells as previously described (Bauss et al, 2014; Sorusch et al, 2017). PLAs were performed according to manufacturer´s protocol adapted to our immunohistochemistry protocol, on unfixed cryosections of human retina. Briefly, cryosections were incubated with the primary antibodies (harmonin H3 and a 1:1:1 cocktail of three mAb opsin clones B6-30a1, K16-155, and R2-15) overnight at 4°C and fixed with 2% paraformaldehyde in PBS. After several washes in PBS specimen were incubated with oligonucleotide-labelled secondary antibodies ("PLA probes") for 4 h at 37°C. After

several washing steps hybridizing connector oligonucleotides were added and ligation was performed for 1 hour at 37°C, to form a closed circle template. This was followed by rolling circle amplification for 120 min, addition of fluorescent-labelled oligonucleotides and analysis by fluorescence microscopy. For the negative controls, samples probed with only one protein-specific antibody and paired with either the rabbit or mouse IgG specific oligonucleotide-labelled antibody. Cells were mounted in Mowiol 4.88 (Hoechst) and analyzed with a Leica DM6000B microscope. Analysis was done on four sections. Signals from negative controls got subtracted from signals of the antibody combination.

Rod outer segment preparation. Rod outer segments (ROS) were purified from 5 pig retinae using a method adapted from Papermaster (Papermaster, 1982). Harvested pellets with the ROS was stored at -80°C before use in immunoblot analyses.

Author contributions

KNW and UW conceived and supervised the research project and wrote, reviewed, edited the manuscript. AG, MA and AS supervised bioinformatics. BF generated RNA-seq libraries. BF, TM, MB, MS and AL analyzed RNA-seq data. AG and LK performed and analyzed bulkRNAseq. Data collection and analyses were performed by JS (ciliogenesis). MB, TG, KNW (RT-PCR, PLAs, Western blots, immunohistochemistry, TEM), KAW (Western blots), DS, BG, and JR (Co-IP, pull-downs) and KF (ROS purification). KS and SK provided human skin biopsies and generation of dermal primary fibroblast. KS did clinical examination of USH1C patients. MA, JMV and NP provided human donor eyes. Data were discussed with all coauthors.

Acknowledgments.

We wish to thank Ulrike Maas, Elisabeth Sehn, and Gabriele B. Stern-Schneider for their excellent technical assistance. This work was supported by FAUN Foundation (Nuremberg) (UW, KNW), USHER2020 (UW, KNW), the Foundation Fighting Blindness (FFB PPA-0717-0719-RAD) (UW, KNW), the German Research Council/DFG in the framework of the SPP SPP2127 - Gene and Cell based therapies to counteract neuroretinal degeneration: NA1398/1-1 (KNW), GR4403/5-1 (AG), KO2176/3-1 (SK), …. (ST), WO548/9-1 (UW), European Union Seventh Framework Program under the grant agreements 242013 (TREATRUSH) (UW) and 241955 (SYSCILIA) (UW), ProRetina Foundation Germany (Pro-Re/Seed/Kaplan-Grosche.8-2019) (AG) and NEI-IRP ZIAEY000546 (AS).

Conflict of interest

Authors declare no conflict of interest.

References

Adamus G, Zam ZS, Arendt A, Palczewski K, McDowell JH, Hargrave PA (1991) Anti-rhodopsin monoclonal antibodies of defined specificity: characterization and application. *Vision Res* **31:** 17-31

Adato A, Michel V, Kikkawa Y, Reiners J, Alagramam KN, Weil D, Yonekawa H, Wolfrum U, El-Amraoui A, Petit C (2005) Interactions in the network of Usher syndrome type 1 proteins. *Hum Mol Genet* **14:** 347-356

Ahmed ZM, Jaworek TJ, Sarangdhar GN, Zheng L, Gul K, Khan SN, Friedman TB, Sisk RA, Bartles JR, Riazuddin S, Riazuddin S (2018) Inframe deletion of human ESPN is associated with deafness, vestibulopathy and vision impairment. *J Med Genet* **55:** 479-488

Bahloul A, Michel V, Hardelin JP, Nouaille S, Hoos S, Houdusse A, England P, Petit C (2010) Cadherin-23, myosin VIIa and harmonin, encoded by Usher syndrome type I genes, form a ternary complex and interact with membrane phospholipids. *Hum Mol Genet* **19:** 3557-3565

Bauss K, Knapp B, Jores P, Roepman R, Kremer H, Wijk EV, Marker T, Wolfrum U (2014) Phosphorylation of the Usher syndrome 1G protein SANS controls Magi2-mediated endocytosis. *Hum Mol Genet* **23:** 3923-3942

Blanks JC, Johnson LV (1984) Specific binding of peanut lectin to a class of retinal photoreceptor cells. A species comparison. *Invest Ophthalmol Vis Sci* **25:** 546-557

Boeda B, El-Amraoui A, Bahloul A, Goodyear R, Daviet L, Blanchard S, Perfettini I, Fath KR, Shorte S, Reiners J, Houdusse A, Legrain P, Wolfrum U, Richardson G, Petit C (2002) Myosin VIIa, harmonin and cadherin 23, three Usher I gene products that cooperate to shape the sensory hair cell bundle. *EMBO J* **21:** 6689-6699

Bolger AM, Lohse M, Usadel B (2014) Trimmomatic: a flexible trimmer for Illumina sequence data. *Bioinformatics* **30:** 2114-2120

Booth KT, Kahrizi K, Babanejad M, Daghagh H, Bademci G, Arzhangi S, Zareabdollahi D, Duman D, El-Amraoui A, Tekin M, Najmabadi H, Azaiez H, Smith RJ (2018) Variants in CIB2 cause DFNB48 and not USH1J. *Clin Genet* **93:** 812-821

Bray NL, Pimentel H, Melsted P, Pachter L (2016) Near-optimal probabilistic RNA-seq quantification. *Nat Biotechnol* **34:** 525-527

Bringmann A, Pannicke T, Grosche J, Francke M, Wiedemann P, Skatchkov SN, Osborne NN, Reichenbach A (2006) Muller cells in the healthy and diseased retina. *Prog Retin Eye Res* **25:** 397-424

Bujakowska KM, Liu Q, Pierce EA (2017) Photoreceptor Cilia and Retinal Ciliopathies. *Cold Spring Harb Perspect Biol*

Burgoyne T, Meschede IP, Burden JJ, Bailly M, Seabra MC, Futter CE (2015) Rod disc renewal occurs by evagination of the ciliary plasma membrane that makes cadherin-based contacts with the inner segment. *Proc Natl Acad Sci U S A* **112:** 15922-15927

Corral-Serrano JC, Lamers IJC, van Reeuwijk J, Duijkers L, Hoogendoorn ADM, Yildirim A, Argyrou N, Ruigrok RAA, Letteboer SJF, Butcher R, van Essen MD, Sakami S, van Beersum SEC, Palczewski K, Cheetham ME, Liu Q, Boldt K, Wolfrum U, Ueffing M, Garanto A, Roepman R, Collin RWJ (2020) PCARE and WASF3 regulate ciliary F-actin assembly that is required for the initiation of photoreceptor outer segment disk formation. *Proc Natl Acad Sci U S A* **117:** 9922-9931

Cowan CS, Renner M, De Gennaro M, Gross-Scherf B, Goldblum D, Hou Y, Munz M, Rodrigues TM, Krol J, Szikra T, Cuttat R, Waldt A, Papasaikas P, Diggelmann R, Patino-

Alvarez CP, Galliker P, Spirig SE, Pavlinic D, Gerber-Hollbach N, Schuierer S, Srdanovic A, Balogh M, Panero R, Kusnyerik A, Szabo A, Stadler MB, Orgul S, Picelli S, Hasler PW, Hierlemann A, Scholl HPN, Roma G, Nigsch F, Roska B (2020) Cell Types of the Human Retina and Its Organoids at Single-Cell Resolution. *Cell* **182:** 1623-1640 e1634

Crawley SW, Shifrin DA, Jr., Grega-Larson NE, McConnell RE, Benesh AE, Mao S, Zheng Y, Zheng QY, Nam KT, Millis BA, Kachar B, Tyska MJ (2014) Intestinal brush border assembly driven by protocadherin-based intermicrovillar adhesion. *Cell* **157:** 433-446

Daniele LL, Adams RH, Durante DE, Pugh EN, Jr., Philp NJ (2007) Novel distribution of junctional adhesion molecule-C in the neural retina and retinal pigment epithelium. *J Comp Neurol* **505:** 166-176

Dobin A, Davis CA, Schlesinger F, Drenkow J, Zaleski C, Jha S, Batut P, Chaisson M, Gingeras TR (2013) STAR: ultrafast universal RNA-seq aligner. *Bioinformatics* **29:** 15-21

DuChez BJ, Hueschen CL, Zimmerman SP, Baumer Y, Wincovitch S, Playford MP (2019) Characterization of the interaction between beta-catenin and sorting nexin 27: contribution of the type I PDZ-binding motif to Wnt signaling. *Biosci Rep* **39**

Ebnet K, Aurrand-Lions M, Kuhn A, Kiefer F, Butz S, Zander K, Meyer zu Brickwedde MK, Suzuki A, Imhof BA, Vestweber D (2003) The junctional adhesion molecule (JAM) family members JAM-2 and JAM-3 associate with the cell polarity protein PAR-3: a possible role for JAMs in endothelial cell polarity. *J Cell Sci* **116:** 3879-3891

El-Amraoui A, Petit C (2005) Usher I syndrome: unravelling the mechanisms that underlie the cohesion of the growing hair bundle in inner ear sensory cells. *J Cell Sci* **118:** 4593-4603

Fadl BR, Brodie SA, Malasky M, Boland JF, Kelly MC, Kelley MW, Boger E, Fariss R, Swaroop A, Campello L (2020) An optimized protocol for retina single-cell RNA sequencing. *Mol Vis* **26:** 705-717

Friedman TB, Schultz JM, Ahmed ZM, Tsilou ET, Brewer CC (2011) Usher syndrome: hearing loss with vision loss. *Adv Otorhinolaryngol* **70:** 56-65

Fuster-Garcia C, Garcia-Bohorquez B, Rodriguez-Munoz A, Aller E, Jaijo T, Millan JM, Garcia-Garcia G (2021) Usher Syndrome: Genetics of a Human Ciliopathy. *Int J Mol Sci* **22**

Gao H, A L, Huang X, Chen X, Xu H (2021) Muller Glia-Mediated Retinal Regeneration. *Mol Neurobiol* **58:** 2342-2361

Goldberg AF, Moritz OL, Williams DS (2016) Molecular basis for photoreceptor outer segment architecture. *Prog Retin Eye Res* **55:** 52-81

Golenhofen N, Drenckhahn D (2000) The catenin, p120ctn, is a common membrane-associated protein in various epithelial and non-epithelial cells and tissues. *Histochem Cell Biol* **114:** 147-155

Gregory FD, Bryan KE, Pangrsic T, Calin-Jageman IE, Moser T, Lee A (2011) Harmonin inhibits presynaptic Cav1.3 Ca(2)(+) channels in mouse inner hair cells. *Nat Neurosci* **14:** 1109-1111

Gregory FD, Pangrsic T, Calin-Jageman IE, Moser T, Lee A (2013) Harmonin enhances voltage-dependent facilitation of Cav1.3 channels and synchronous exocytosis in mouse inner hair cells. *J Physiol* **591:** 3253-3269

Grillet N, Xiong W, Reynolds A, Kazmierczak P, Sato T, Lillo C, Dumont RA, Hintermann E, Sczaniecka A, Schwander M, Williams D, Kachar B, Gillespie PG, Muller U (2009) Harmonin mutations cause mechanotransduction defects in cochlear hair cells. *Neuron* **62:** 375-387

Grosche A, Hauser A, Lepper MF, Mayo R, von Toerne C, Merl-Pham J, Hauck SM (2016) The Proteome of Native Adult Muller Glial Cells From Murine Retina. *Mol Cell Proteomics* **15:** 462-480

Grotz S, Schäfer J, Wunderlich KA, Ellederova Z, Auch H, Bähr A, Runa-Vochozkova P, Plutniok J, Arnold V, Ardan T, Veith M, Santamaria G, Dhom G, Hitzl W, Kessler B, Kurome M, Zakharchenko V, Linnert J, Fischer A, Blutke A, Döring A, Suchankova S,

Popelar J, May-Simera H, Laugwitz KL, Vandenberghe LH, Wolf E, Nagel-Wolfrum K, Motlik J, Fischer MD, Wolfrum U, Klymiuk N (2021) Early Disruption of Photoreceptor Cell Architecture and Loss of Vision in a Humanized Pig Model of Usher Syndrome. bioRxiv doi: https://doi.org/10.1101/2021.05.31.446123

Hosoi N, Arai I, Tachibana M (2005) Group III metabotropic glutamate receptors and exocytosed protons inhibit L-type calcium currents in cones but not in rods. *J Neurosci* **25:** 4062-4072

Kersten FF, van Wijk E, van Reeuwijk J, van der Zwaag B, Marker T, Peters TA, Katsanis N, Wolfrum U, Keunen JE, Roepman R, Kremer H (2010) Association of whirlin with Cav1.3 (alpha1D) channels in photoreceptors, defining a novel member of the usher protein network. *Invest Ophthalmol Vis Sci* **51:** 2338-2346

Kim E, Sheng M (2004) PDZ domain proteins of synapses. *Nat Rev Neurosci* **5:** 771-781

Kimberling WJ, Hildebrand MS, Shearer AE, Jensen ML, Halder JA, Trzupek K, Cohn ES, Weleber RG, Stone EM, Smith RJ (2010) Frequency of Usher syndrome in two pediatric populations: Implications for genetic screening of deaf and hard of hearing children. *Genet Med* **12:** 512-516

Kremer H, van Wijk E, Marker T, Wolfrum U, Roepman R (2006) Usher syndrome: molecular links of pathogenesis, proteins and pathways. *Hum Mol Genet* **15 Spec No 2:** R262-270

Li B, Dewey CN (2011) RSEM: accurate transcript quantification from RNA-Seq data with or without a reference genome. *BMC Bioinformatics* **12:** 323

Li H, Handsaker B, Wysoker A, Fennell T, Ruan J, Homer N, Marth G, Abecasis G, Durbin R, Genome Project Data Processing S (2009) The Sequence Alignment/Map format and SAMtools. *Bioinformatics* **25:** 2078-2079

Li J, He Y, Lu Q, Zhang M (2016) Mechanistic Basis of Organization of the Harmonin/USH1C-Mediated Brush Border Microvilli Tip-Link Complex. *Dev Cell* **36:** 179-189

Ling JP, Wilks C, Charles R, Leavey PJ, Ghosh D, Jiang L, Santiago CP, Pang B, Venkataraman A, Clark BS, Nellore A, Langmead B, Blackshaw S (2020) ASCOT identifies key regulators of neuronal subtype-specific splicing. *Nat Commun* **11:** 137

Lodha N, Bonfield S, Orton NC, Doering CJ, McRory JE, Mema SC, Rehak R, Sauve Y, Tobias R, Stell WK, Bech-Hansen NT (2010) Congenital stationary night blindness in mice - a tale of two Cacna1f mutants. *Adv Exp Med Biol* **664:** 549-558

Lodha N, Loucks CM, Beaulieu C, Parboosingh JS, Bech-Hansen NT (2012) Congenital stationary night blindness: mutation update and clinical variability. *Adv Exp Med Biol* **723:** 371-379

Maerker T, van Wijk E, Overlack N, Kersten FF, McGee J, Goldmann T, Sehn E, Roepman R, Walsh EJ, Kremer H, Wolfrum U (2008) A novel Usher protein network at the periciliary reloading point between molecular transport machineries in vertebrate photoreceptor cells. *Hum Mol Genet* **17:** 71-86

Mathur P, Yang J (2015) Usher syndrome: Hearing loss, retinal degeneration and associated abnormalities. *Biochim Biophys Acta* **1852:** 406-420

May-Simera H, Nagel-Wolfrum K, Wolfrum U (2017) Cilia - The sensory antennae in the eye. *Prog Retin Eye Res* **60:** 144-180

Michel V, Booth KT, Patni P, Cortese M, Azaiez H, Bahloul A, Kahrizi K, Labbe M, Emptoz A, Lelli A, Degardin J, Dupont T, Aghaie A, Oficjalska-Pham D, Picaud S, Najmabadi H, Smith RJ, Bowl MR, Brown SD, Avan P, Petit C, El-Amraoui A (2017) CIB2, defective in isolated deafness, is key for auditory hair cell mechanotransduction and survival. *EMBO Mol Med* **9:** 1711-1731

Millan JM, Aller E, Jaijo T, Blanco-Kelly F, Gimenez-Pardo A, Ayuso C (2011) An update on the genetics of usher syndrome. *J Ophthalmol* **2011:** 417217

Montell C (1999) Visual transduction in Drosophila. *Annu Rev Cell Dev Biol* **15:** 231-268

Murphy D, Cieply B, Carstens R, Ramamurthy V, Stoilov P (2016) The Musashi 1 Controls the Splicing of Photoreceptor-Specific Exons in the Vertebrate Retina. *PLoS Genet* **12:** e1006256

Nagel-Wolfrum K, Moller F, Penner I, Wolfrum U (2014) Translational read-through as an alternative approach for ocular gene therapy of retinal dystrophies caused by in-frame nonsense mutations. *Vis Neurosci* **31:** 309-316

Omri S, Omri B, Savoldelli M, Jonet L, Thillaye-Goldenberg B, Thuret G, Gain P, Jeanny JC, Crisanti P, Behar-Cohen F (2010) The outer limiting membrane (OLM) revisited: clinical implications. *Clin Ophthalmol* **4:** 183-195

Papermaster DS (1982) Preparation of retinal rod outer segments. *Methods Enzymol* **81:** 48-52

Phillips JB, Blanco-Sanchez B, Lentz JJ, Tallafuss A, Khanobdee K, Sampath S, Jacobs ZG, Han PF, Mishra M, Titus TA, Williams DS, Keats BJ, Washbourne P, Westerfield M (2011) Harmonin (Ush1c) is required in zebrafish Muller glial cells for photoreceptor synaptic development and function. *Dis Model Mech* **4:** 786-800

Pinelli M, Carissimo A, Cutillo L, Lai CH, Mutarelli M, Moretti MN, Singh MV, Karali M, Carrella D, Pizzo M, Russo F, Ferrari S, Ponzin D, Angelini C, Banfi S, di Bernardo D (2016) An atlas of gene expression and gene co-regulation in the human retina. *Nucleic Acids Res* **44:** 5773-5784

Pinette JA, Mao S, Millis BA, Krystofiak ES, Faust JJ, Tyska MJ (2019) Brush border protocadherin CDHR2 promotes the elongation and maximized packing of microvilli in vivo. *Mol Biol Cell* **30:** 108-118

Rafizadeh S, Zhang Z, Woltz RL, Kim HJ, Myers RE, Lu L, Tuteja D, Singapuri A, Bigdeli AA, Harchache SB, Knowlton AA, Yarov-Yarovoy V, Yamoah EN, Chiamvimonvat N (2014) Functional interaction with filamin A and intracellular Ca2+ enhance the surface membrane expression of a small-conductance Ca2+-activated K+ (SK2) channel. *Proc Natl Acad Sci U S A* **111:** 9989-9994

Reiners J, Nagel-Wolfrum K, Jurgens K, Marker T, Wolfrum U (2006) Molecular basis of human Usher syndrome: deciphering the meshes of the Usher protein network provides insights into the pathomechanisms of the Usher disease. *Exp Eye Res* **83:** 97-119

Reiners J, Reidel B, El-Amraoui A, Boeda B, Huber I, Petit C, Wolfrum U (2003) Differential distribution of harmonin isoforms and their possible role in Usher-1 protein complexes in mammalian photoreceptor cells. *Invest Ophthalmol Vis Sci* **44:** 5006-5015

Reiners J, van Wijk E, Marker T, Zimmermann U, Jurgens K, te Brinke H, Overlack N, Roepman R, Knipper M, Kremer H, Wolfrum U (2005) Scaffold protein harmonin (USH1C) provides molecular links between Usher syndrome type 1 and type 2. *Hum Mol Genet* **14:** 3933-3943

Riazuddin S, Belyantseva IA, Giese AP, Lee K, Indzhykulian AA, Nandamuri SP, Yousaf R, Sinha GP, Lee S, Terrell D, Hegde RS, Ali RA, Anwar S, Andrade-Elizondo PB, Sirmaci A, Parise LV, Basit S, Wali A, Ayub M, Ansar M, Ahmad W, Khan SN, Akram J, Tekin M, Riazuddin S, Cook T, Buschbeck EK, Frolenkov GI, Leal SM, Friedman TB, Ahmed ZM (2012) Alterations of the CIB2 calcium- and integrin-binding protein cause Usher syndrome type 1J and nonsyndromic deafness DFNB48. *Nat Genet* **44:** 1265-1271

Robinson JT, Thorvaldsdottir H, Winckler W, Guttman M, Lander ES, Getz G, Mesirov JP (2011) Integrative genomics viewer. *Nat Biotechnol* **29:** 24-26

Rodieck, RW (1998). The first steps in seeing (Vol. 1). Sunderland, MA: Sinauer Associates.

Sahly I, Dufour E, Schietroma C, Michel V, Bahloul A, Perfettini I, Pepermans E, Estivalet A, Carette D, Aghaie A, Ebermann I, Lelli A, Iribarne M, Hardelin JP, Weil D, Sahel JA, El-Amraoui A, Petit C (2012) Localization of Usher 1 proteins to the photoreceptor calyceal processes, which are absent from mice. *J Cell Biol* **199:** 381-399

Samanta A, Stingl K, Kohl S, Ries J, Linnert J, Nagel-Wolfrum K (2019) Ataluren for the Treatment of Usher Syndrome 2A Caused by Nonsense Mutations. *Int J Mol Sci* **20**

Scanlan MJ, Williamson B, Jungbluth A, Stockert E, Arden KC, Viars CS, Gure AO, Gordan JD, Chen YT, Old LJ (1999) Isoforms of the human PDZ-73 protein exhibit differential tissue expression. *Biochim Biophys Acta* **1445:** 39-52

Schafer N, Grosche A, Schmitt SI, Braunger BM, Pauly D (2017) Complement Components Showed a Time-Dependent Local Expression Pattern in Constant and Acute White Light-Induced Photoreceptor Damage. *Front Mol Neurosci* **10:** 197

Schietroma C, Parain K, Estivalet A, Aghaie A, Boutet de Monvel J, Picaud S, Sahel JA, Perron M, El-Amraoui A, Petit C (2017) Usher syndrome type 1-associated cadherins shape the photoreceptor outer segment. *J Cell Biol* **216:** 1849-1864

Sedmak T, Sehn E, Wolfrum U (2009) Immunoelectron microscopy of vesicle transport to the primary cilium of photoreceptor cells. *Methods Cell Biol* **94:** 259-272

Sorusch N, Bauss K, Plutniok J, Samanta A, Knapp B, Nagel-Wolfrum K, Wolfrum U (2017) Characterization of the ternary Usher syndrome SANS/ush2a/whirlin protein complex. *Hum Mol Genet* **26(6)**: 1157-1172.

Spencer WJ, Lewis TR, Pearring JN, Arshavsky VY (2020) Photoreceptor Discs: Built Like Ectosomes. *Trends Cell Biol* **30:** 904-915

Sturm D (2020) Generation and functional characterization of USH1C isoform harmonin a1 lacking exon 3. Master Thesis, Faculty of Biology, JGU Mainz

Sundar J, Matalkah F, Jeong B, Stoilov P, Ramamurthy V (2021) The Musashi proteins MSI1 and MSI2 are required for photoreceptor morphogenesis and vision in mice. *J Biol Chem* **296:** 100048

Testa F, Melillo P, Bonnet C, Marcelli V, de Benedictis A, Colucci R, Gallo B, Kurtenbach A, Rossi S, Marciano E, Auricchio A, Petit C, Zrenner E, Simonelli F (2017) Clinical Presentation and Disease Course of Usher Syndrome Because of Mutations in Myo7a or Ush2a. *Retina* **37:** 1581-1590

Thorvaldsdottir H, Robinson JT, Mesirov JP (2013) Integrative Genomics Viewer (IGV): high-performance genomics data visualization and exploration. *Brief Bioinform* **14:** 178-192

tom Dieck S, Brandstatter JH (2006) Ribbon synapses of the retina. *Cell Tissue Res* **326:** 339-346

Verpy E, Leibovici M, Zwaenepoel I, Liu XZ, Gal A, Salem N, Mansour A, Blanchard S, Kobayashi I, Keats BJ, Slim R, Petit C (2000) A defect in harmonin, a PDZ domain-containing protein expressed in the inner ear sensory hair cells, underlies Usher syndrome type 1C. *Nat Genet* **26:** 51-55

Vogel C, Marcotte EM (2012) Insights into the regulation of protein abundance from proteomic and transcriptomic analyses. *Nat Rev Genet* **13:** 227-232

Weibrecht I, Leuchowius KJ, Clausson CM, Conze T, Jarvius M, Howell WM, Kamali-Moghaddam M, Soderberg O (2010) Proximity ligation assays: a recent addition to the proteomics toolbox. *Expert Rev Proteomics* **7:** 401-409

Williams DS (2008) Usher syndrome: animal models, retinal function of Usher proteins, and prospects for gene therapy. *Vision Res* **48:** 433-441

Williams DS, Aleman TS, Lillo C, Lopes VS, Hughes LC, Stone EM, Jacobson SG (2009) Harmonin in the murine retina and the retinal phenotypes of Ush1c-mutant mice and human USH1C. *Invest Ophthalmol Vis Sci* **50:** 3881-3889

Wolfrum U (1991) Centrin-Like and Alpha-Actinin-Like Immunoreactivity in the Ciliary Rootlets of Insect Sensilla. *Cell and Tissue Research* **266:** 231-238

Wolfrum U, Goldmann T, Overlack N, Mueller C, Vetter JM, Nagel-Wolfrum K (2010) Subcellular Localization of Usher Syndrome Proteins in the Human Retina. *Invest Ophthalmol Vis Sci* **51:** 2494-2494

Wolfrum U, Schmitt A (2000) Rhodopsin transport in the membrane of the connecting cilium of mammalian photoreceptor cells. *Cell Motil Cytoskeleton* **46:** 95-107

Wu L, Pan L, Zhang C, Zhang M (2012) Large protein assemblies formed by multivalent interactions between cadherin23 and harmonin suggest a stable anchorage structure at the tip link of stereocilia. *J Biol Chem* **287:** 33460-33471

Xu L, Bolch SN, Santiago CP, Dyka FM, Akil O, Lobanova ES, Wang Y, Martemyanov KA, Hauswirth WW, Smith WC, Handa JT, Blackshaw S, Ash JD, Dinculescu A (2020) Clarin-1 expression in adult mouse and human retina highlights a role of Muller glia in Usher syndrome. *J Pathol* **250:** 195-204

Xu XZ, Choudhury A, Li X, Montell C (1998) Coordination of an array of signaling proteins through homo- and heteromeric interactions between PDZ domains and target proteins. *J Cell Biol* **142:** 545-555

Yan D, Li F, Hall ML, Sage C, Hu WH, Giallourakis C, Upadhyay G, Ouyang XM, Du LL, Bethea JR, Chen ZY, Yajnik V, Liu XZ (2006) An isoform of GTPase regulator DOCK4 localizes to the stereocilia in the inner ear and binds to harmonin (USH1C). *J Mol Biol* **357:** 755-764

Yan J, Pan L, Chen X, Wu L, Zhang M (2010) The structure of the harmonin/sans complex reveals an unexpected interaction mode of the two Usher syndrome proteins. *Proc Natl Acad Sci U S A* **107:** 4040-4045

Yildirim A, Mozaffari-Jovin S, Wallisch AK, Schafer J, Ludwig SEJ, Urlaub H, Luhrmann R, Wolfrum U (2021) SANS (USH1G) regulates pre-mRNA splicing by mediating the intra-nuclear transfer of tri-snRNP complexes. *Nucleic Acids Res* **49:** 5845-5866

Zwaenepoel I, Verpy E, Blanchard S, Meins M, Apfelstedt-Sylla E, Gal A, Petit C (2001) Identification of three novel mutations in the USH1C gene and detection of thirty-one polymorphisms used for haplotype analysis. *Hum Mutat* **17:** 34-41

Figures with legends

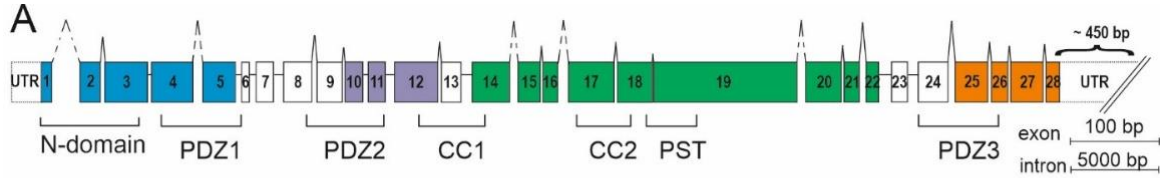

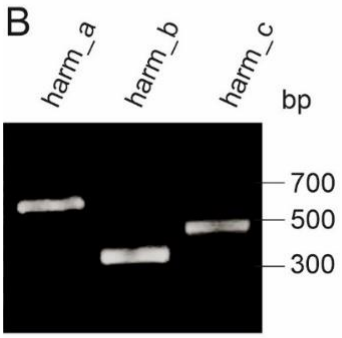

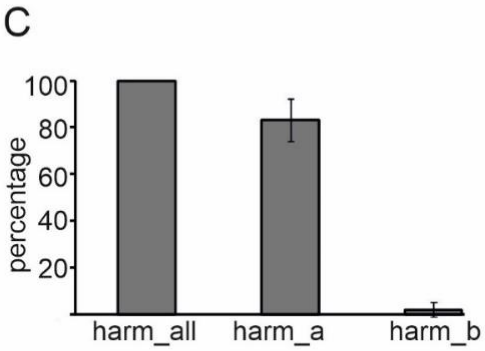

D

donor	a	b
220	86.74	4.07
252	76.21	0.18
263	86.51	2.06
mean	83.15	2.10

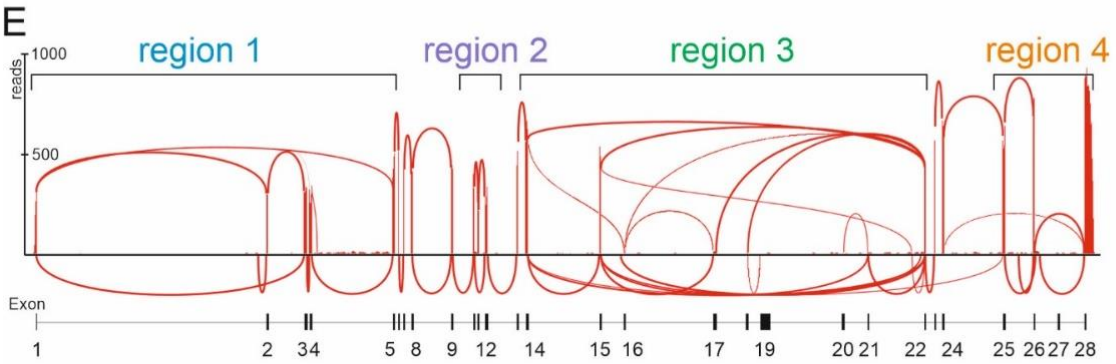

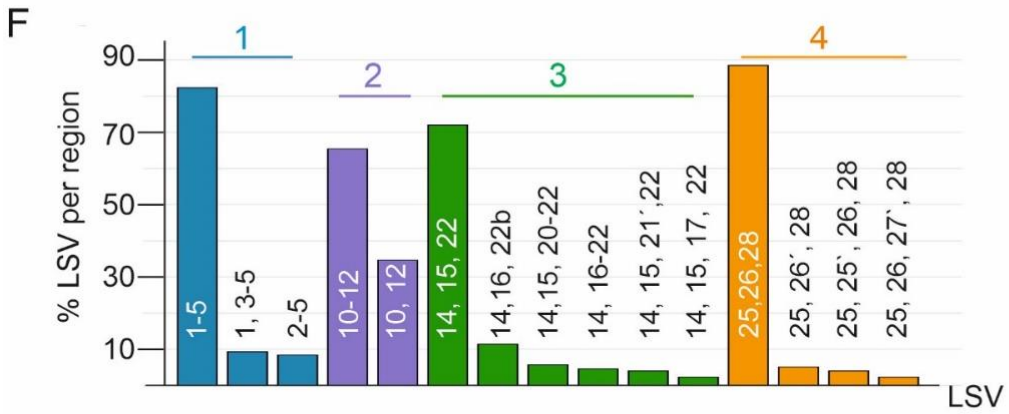

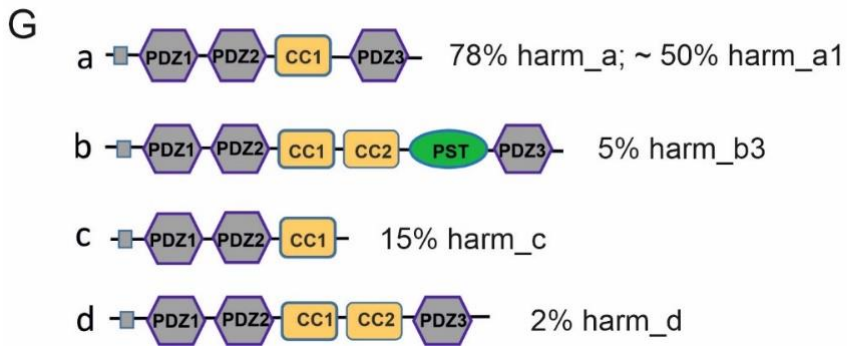

Figure 1. Expression of *USH1C*/harmonin a, b and c transcripts in the human retina.

(**A**) Exon and intron structure of human *USH1C*. Exons are shown in boxes and denoted by the numbers from 1 to 28. The different domains of the harmonin protein, namely PDZ (PSD-95, DLG, ZO-1), PST ((proline-serine-threonine rich), cc (coiled-coil), are marked by brackets below the gene structure. Colours indicate regions of local splice variant (LSV) analyses (see, E and F) (**B-D**) Three independent RT-PCR analysis of *USH1C*/harmonin transcripts using isoform specific primers in human retina. The RNA used for RT-PCR analyses was derived from human adult retina. (**B**) RT-PCR analysis of *USH1C*/harmonin transcripts using isoform specific primers in human retina. Transcripts of *USH1C*/harmonin isoforms a, b and c were detected (**C**) Quantitative RT-PCR of *USH1C*/harmonin isoforms. Primers detect either all *USH1C*/harmonin transcripts (a, b and c) or are specific for *USH1C*/harmonin a or *USH1C*/harmonin b transcripts, respectively. *USH1C*/harmonin a isoforms are most prominent, while *USH1C*/harmonin b isoforms are rarely expressed. (**D**) Percentages of transcripts in three different human donors is shown. *USH1C*/harmonin a-transcripts were most abundant (83.15%), while *USH1C*/harmonin b-transcripts were barely detected (2.1%). **(E)** Representative Sashimi blot of RNA-seq analysis of human retina. Splicing events were grouped into four regions (region 1 -4). **(F)** Quantification of local splice variants (LSV). LSVs of the same region are depicted in same color. (**G)** Predicted domain structure of the *USH1C*/harmonin transcripts. Percentage of transcripts is based the copy number of LSVs in regions 1-4. *USH1C*/harmonin class a is the most abundant isoform class with *USH1C*/ harmonin a1 being the most expressed isoform.

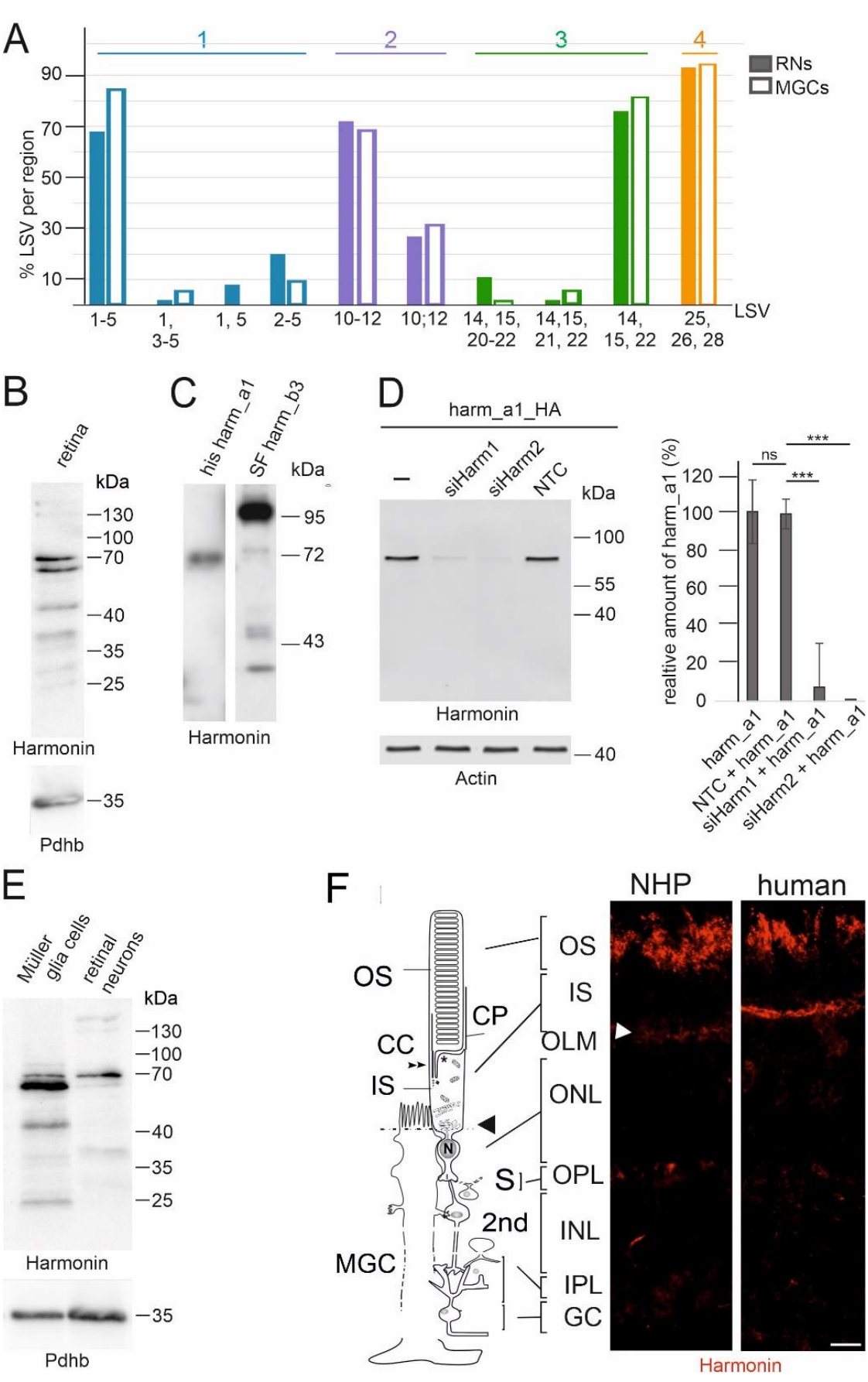

Figure 2. *USH1C*/harmonin expression in retinal cells.

(**A**) BulkRNA-seq of human retinal neurons (RNs) and Müller glial cells (MGCs). In RNs (filled bars) and MGCs (white-coloured bars) *USH1C*/harmonin transcripts are detectable (**B**) Western blot analysis of harmonin protein expression in human retina with affinity-purified polyclonal antibodies against harmonin (H3). (**C**) His-tagged harmonin a1 and SF-tagged harmonin b3 transiently expressed in HEK293T cells. Pan anti-harmonin H3 detected bands which co-migrate at the molecular weights of recombinant harmonin a1. Lower bands which may represent harmonin_c isoforms or degraded products of harmonin_a and/or b. (**D**) Western blot analysis to validate the specificity of the harmonin antibody. A strong harmonin band is detected in HEK293T cells transfected with HA-tagged harmonin (Harm_a1_HA) or co-transfected with Harm_a1_HA and control siRNA (NTC). Harmonin is not detected in cells co-transfected with HA-tagged Harmonin a1 (Harm_a1_HA) and siHarm no harmonin, indicating the specificity of the harmonin antibody. P values: ***: < 0.001. (**E**) Western blot analysis of MGCs and retinal neurons (RNs) isolated from human retina. Both MGCs and RNs express various harmonin isoforms. (**F**) Localization of harmonin in retina sections. Indirect immunofluorescence labelling of harmonin in a longitudinal section through the photoreceptor layer, the outer segments (OS), the inner segments (IS) and the nuclei in the outer nuclear layer (ONL) and Müller glia cells (MGC) of a non-human primate (NHP) and human retina, respectively. In addition to the prominent labelling of the outer limiting membrane (OLM, arrowhead), patchy harmonin staining was present in the layer of the photoreceptor OS. Faint staining was present in the IS, the outer plexiform layer (OPL), the inner plexiform layer (IPL) and ganglion cell layer (GCL). Scale bars: 10 µm.

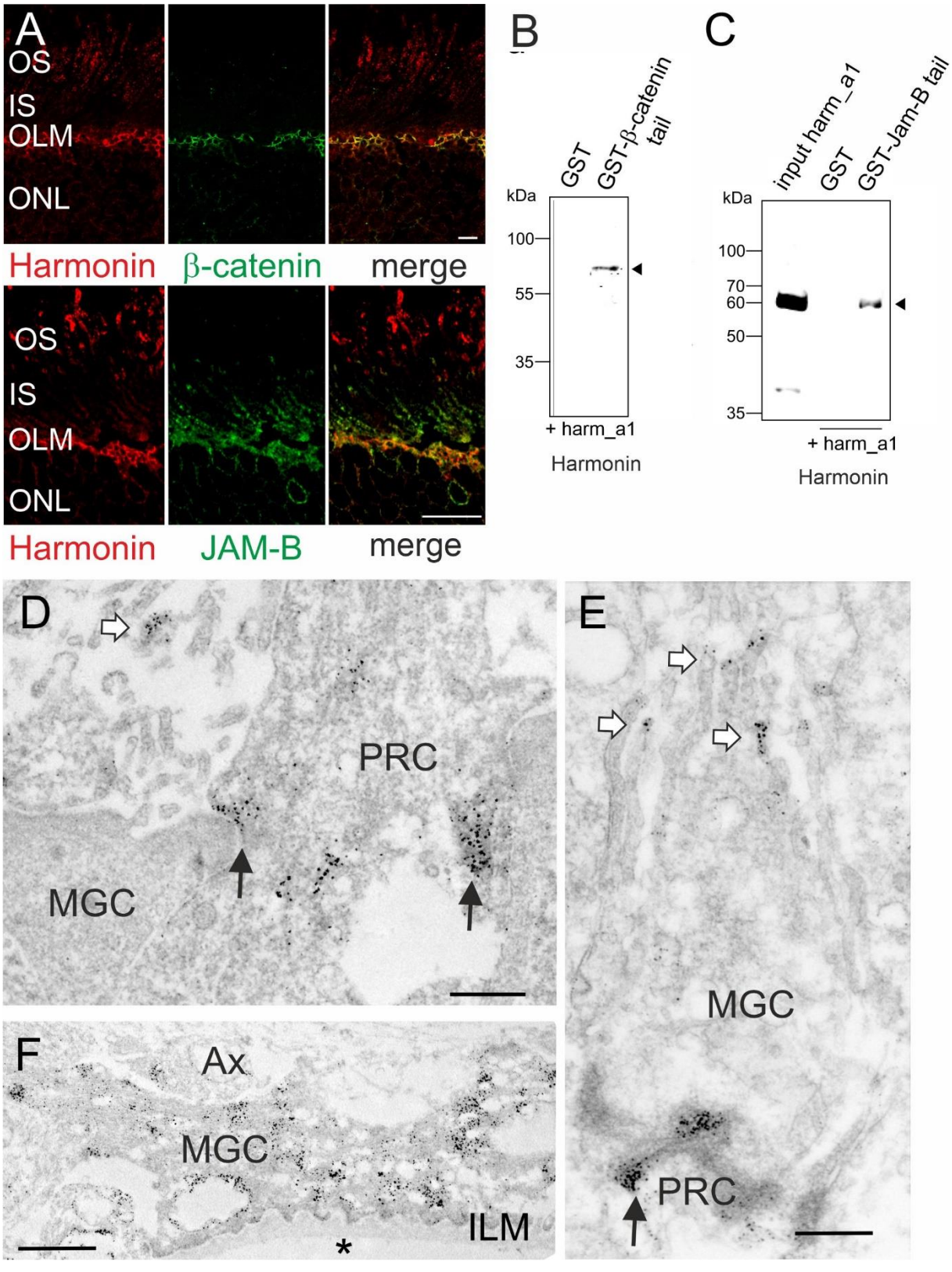

Figure 3. Subcellular harmonin localization at the outer limiting membrane and in Müller glia cells of the human retina.

(**A**) Indirect immunofluorescence double staining of harmonin (red) and the adhesion junction molecule β-catenin (green) or the tight junction molecule JAM-B (green). Merged images demonstrate an overlap of harmonin and β-catenin as well as harmonin and JAM-B localisation at the outer limiting membrane (OLM). (**B, C**) GST-pulldown demonstration the interaction of harmonin a1 (harm a1) with β-catenin tail and JAM-B tail, respectively. (**D**) Immunoelectron microscopy analysis of harmonin labelling in a longitudinal section through the OLM of a human retina. Harmonin labelling concentrated in the electron dense adhesion junctions between Müller glia cells (MGCs) and photoreceptor cells (PRC) in the OLM (black arrows), microvilli of MGCs (white arrows) and MGC endfeet at the inner limiting membrane (ILM) which contacts the vitreous (asterisk). OS, outer segment; IS, inner segment; ONL, outer limiting membrane; AX, axon; Scale bars: β-catenin: 5 µm; JAM-B: 15 µm; D, E: 0.5 µm; F: 1 µm.

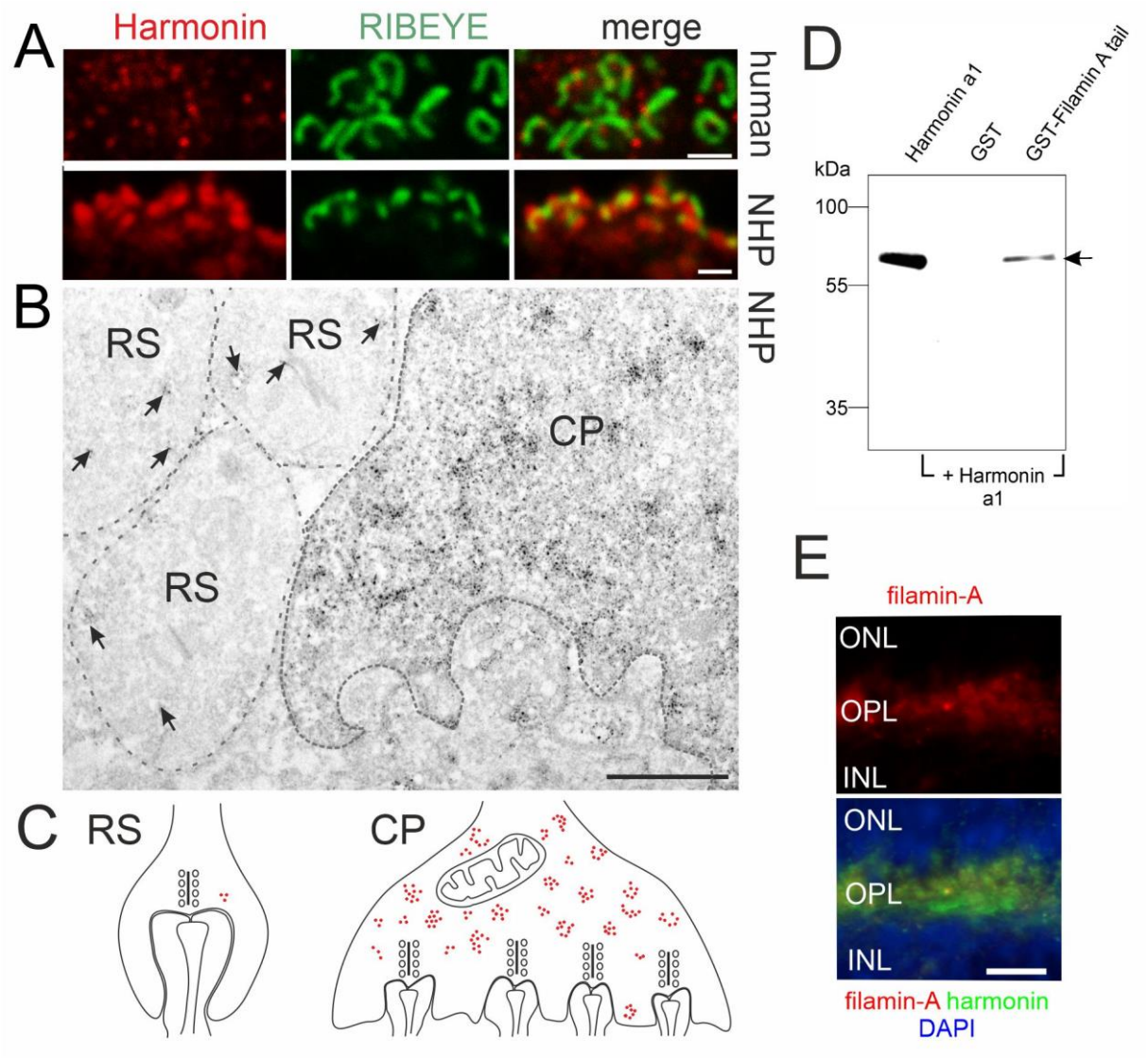

Figure 4 Harmonin localization at primate photoreceptor synapses. (A) Double immunofluorescence labelling of harmonin (red) and pre-synaptic protein RIBEYE (green) in human (upper panel) and non-human primate (NHP, lower panel) outer plexiform layer (OPL) synapses. Merged images revealed co-localization of harmonin and RIBEYE (yellow). (B) Immunoelectron microscopy analysis of harmonin in non-human primate photoreceptor synapses. Dense harmonin labelling was present in cone pedicles (CP), but only weak harmonin labelling (arrows) was observed in rod spherules (RS). (C) Schematic representation of presynaptic harmonin labelling in RS and CP. (D) GST-pull down demonstrate harmonin a1 and filamin-A interaction. (E) Double immunofluorescence labelling of filamin-A (red) and Harmonin in the outer plexiform layer (green). Scale bars: A, B: 1 µm; E: 12 µm

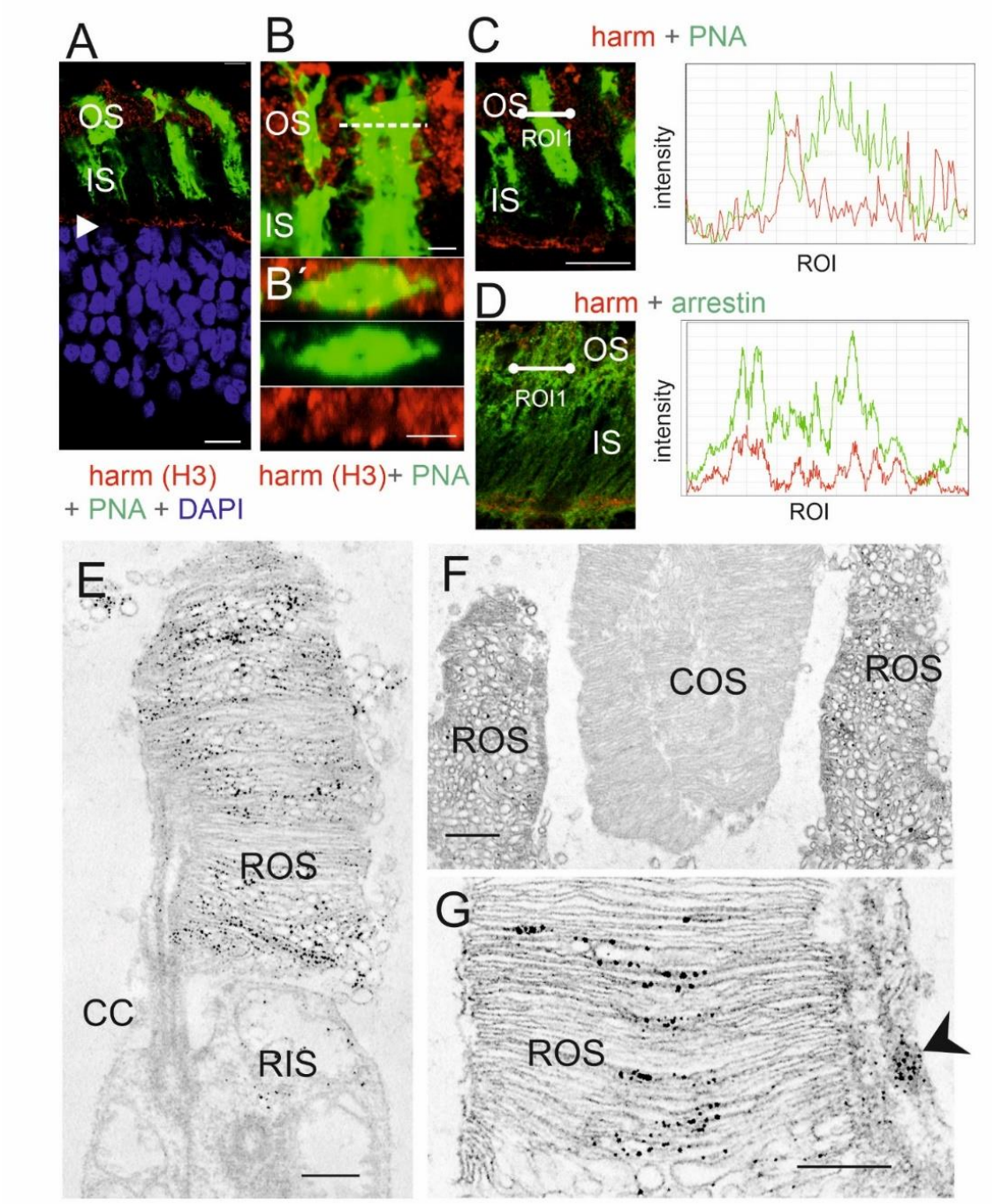

Figure 5. Harmonin in the outer segment of human photoreceptor cells.

(**A**) Merged image of harmonin immunofluorescence (red) and fluorescent peanut agglutinin (PNA, green), a specific marker for the extracellular matrix sheath of cone photoreceptors in a longitudinal section through the photoreceptor layer, the outer segments (OS), the inner segments (IS) and the nuclei in the outer nuclear layer (ONL) of a human retina. In addition to the prominent labelling of the outer limiting membrane (arrowhead) patchy harmonin staining was present in the layer of the photoreceptor OS. (**B, B´**) Magnification of the OS region demonstrate no co-localization of harmonin and PNA (**B´**) Confocal x,y scan image of harmonin and PNA labelling in the photoreceptor layer of a human retina. y, z scan at the dotted line in B at higher magnification. (**C, D**) Double labelling of harmonin (red) with PNA (green) (**C**) and rod-specific arrestin (green) (**D**) in the photoreceptor layer of human retina. Corresponding fluorescence intensity profiles of regions of interest (ROI, white lines) at the right panel demonstrated no co-localization of harmonin and PNA, but co-localization of harmonin and arrestin indicating localization of harmonin in human rod outer segments but not cone outer segments. DAPI (blue): nuclear DNA. (**E-G**) Immunoelectron microscopy labelling of harmonin in a longitudinal section through human retinae. (**E**) In human rod PRCs, harmonin was found in rod outer segments (ROS) and barely detected in rod inner segments (RIS). (**F**) Harmonin was found in ROS, but not in outer segments of cones (COS). (G) Harmonin is detected in ROS and calyceal processes (arrow head). DAPI: blue, nuclear DNA; CC: connecting cilium. Scale bars: A: 10 µm, B: 2.5 µm, B´C, D: 5 µm, E, G: 0.5 µm, F: 1 µm

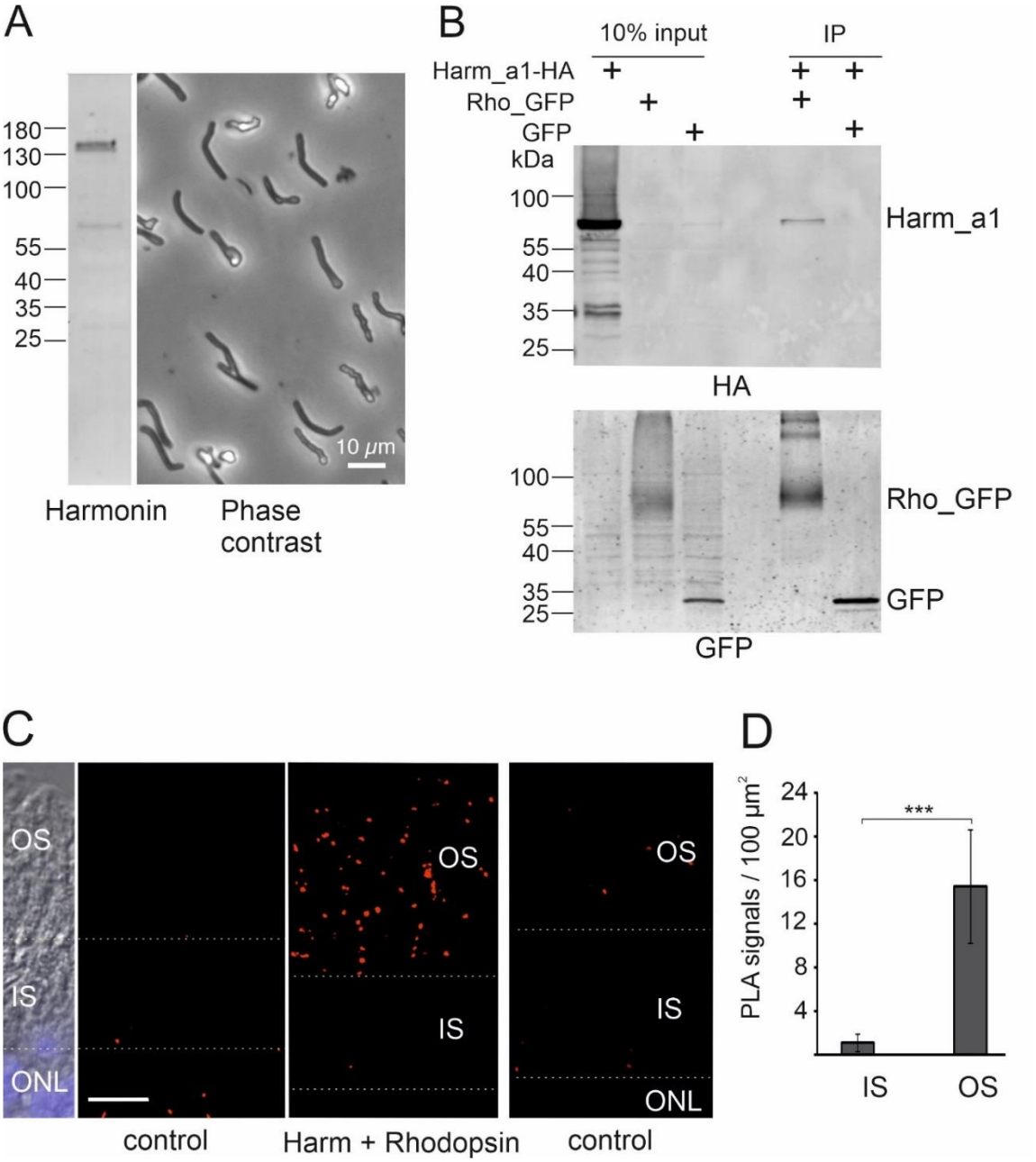

Figure 6. Harmonin is expressed in rod outer segments and interacts with rhodopsin

(**A**) Harmonin is expressed in porcine photoreceptor outer segments. Left panel: Western blot analysis of the isolated porcine outer segment fraction from density gradients revealed harmonin expression. Right panel: phase contrast picture of material used for the Western blot. (**B**) GFP-Trap® demonstrates interaction between harmonin a1 (Harm_a1) and opsin-GFP (Rho_GFP). HEK293T cells were transfected with harmonin_a1-HA-and GFP or opsin-GFP, respectively. Harmonin a1 was precipitated by immobilized opsin-GFP, but not by GFP alone (replicates, n=3) (**C**) Proximity ligation assay (PLA) of harmonin (Harm) and rhodopsin in longitudinal cryosections through a human retina. PLA signals (red dots) reveal close proximity of 40 nm indicating the interaction of harmonin (Harm) and rhodopsin in OS of human PRCs *in situ*. For quantitative analysis the inner segment/outer segment (IS/OS) borders were defined based on DIC images. Nuclear staining by DAPI (blue) was used to define the outer nuclear layer (ONL). ImageJ was adopted to define the different retina layers: OS and IS of PRCs, and ONL (white dashed lines). Control, PLA was performed with anti-opsin only where almost no PLA signal was found. (**D**) Quantification of PLA signals in the OS and IS of PRCs. PLA signals were counted automatically in the different compartments and signals in controls were subtracted in three different samples. The number of PLA signals in OS were also significantly higher when compared to signals in IS. Scale bar: 10 µm.

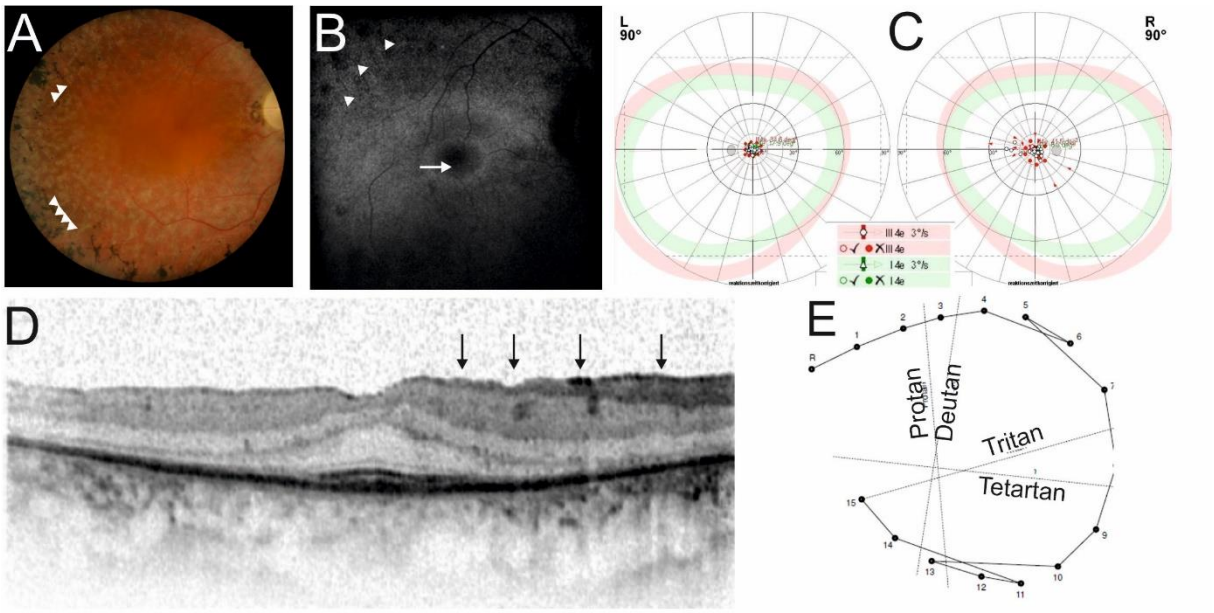

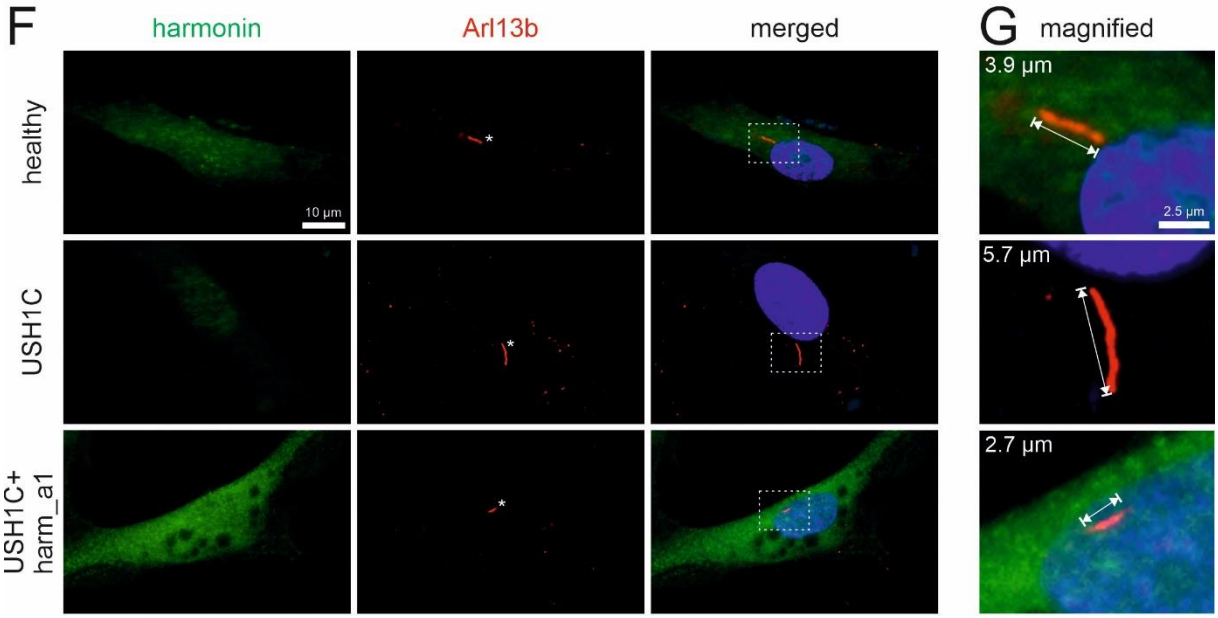

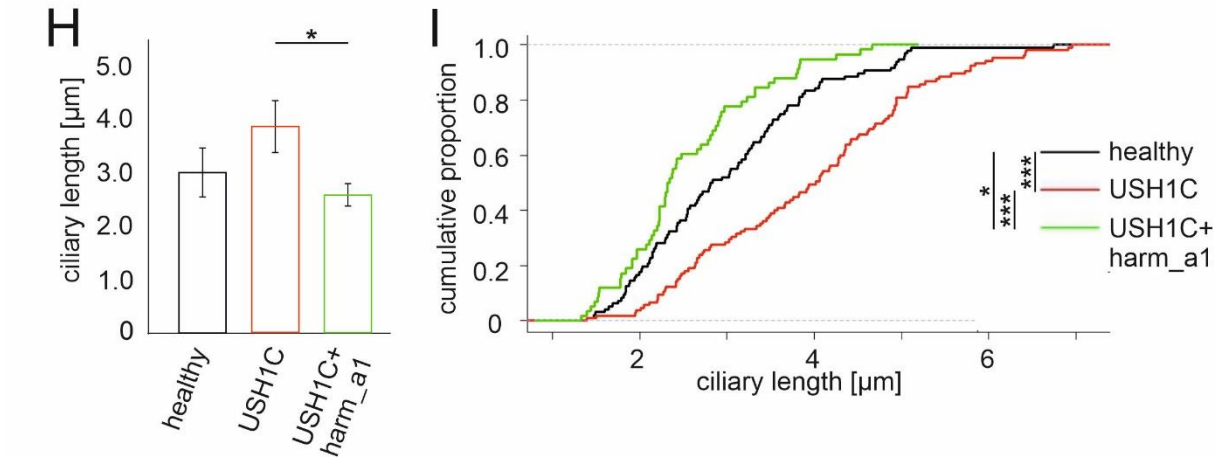

Figure 7. Retina phenotype of an USH1C patient and ciliary phenotype of USH1C patient-derived cells.

(A-E) Clinical findings of the retinal phenotype of a 35-year old male with confirmed mutations in USH1C (c.91C>T;p.(R31*), c.238dupC;p.(Arg80Profs*69))). (**A**) Fundus photography showed bone spiculas in the mid peripheral and peripheral retina (arrow heads), attenuated retinal vessels, waxy pallor optic disc, and white spots of retinal pigment epithelium atrophy. (**B**) Fundus autofluorescence imaging displayed a hyperfluorescence ring around the fovea (arrow) and a disrupted hypofluorescence in the mid- and far periphery of the retina (arrow heads) corresponding to the outer retinal atrophy. (**C**) Kinetic visual field (90°): Concentric constriction for III4e and I4e markers with central preserved area. (D) Optical coherence tomography showed epiretinal gliosis (marked as black vertical arrows), as well as gradual inner segment/outer segment loss up to the fovea. Only the foveal region displays a normal retinal structure with preserved photoreceptors and a central macula thickness 269 µm. (**E**) Lanthony color test showed normal color perception. **(F-I)** Primary ciliary phenotype of USH1C patient-derived cells and rescue by harmonin a1. (**F, G**) Indirect immunofluorescence labelling of harmonin (green) and the ciliary marker Arl13b (red) in fibroblasts of healthy donors (healthy), a patient with confirmed mutations in USH1C (c.91C>T;p.(R31*), 238dupC;p.(Arg80Profs*69)) (USH1C $^{R80Pfs*69/R31*}$), and these USH1C $^{R80Pfs*69/R31*}$ fibroblasts transfected with harmonin a1 (USH1C $^{R80Pfs*69/R31*}$+harm_a1). (**F**) In healthy donor cells and harmonin a1 transfected USH1C $^{R80Pfs*69/R31*}$ cells, harmonin is detectable. In untransfected USH1C $^{R80Pfs*69/R31*}$ cells, harmonin staining is barely visible. (**G-I**) Ciliary length measurements revealed longer cilia in USH1C patient-derived cells compared to control cells (healthy) and harmonin a1 transfected USH1C $^{R80Pfs*69/R31*}$ cells. (**H**) Quantification of the ciliary length. Quantitative analysis of primary ciliary length reveals significant decrease of ciliary length in USH1C+harm_a1 fibroblasts towards the ciliary length of healthy donors (**I**) Cumulative analysis of ciliary length and number of ciliated cells in fibroblasts of healthy donors (healthy), USH1C$^{R80Pfs*69/R31*}$ (USH1C), and USH1C $^{R80Pfs*69/R31*}$ fibroblasts transfected with harmonin a1 (USH1C $^{R80Pfs*69/R31*}$+harm_a1) using R. Two-tailed Student's t test, *p≤0.05, **p≤0.01. Number of cells counted: healthy: n=96; USH1C: n=105; USH1C+harm_a1: 58. Scale bar: F: 10 µm, G: 2.5 µm

Supplementary material

Supplemental Figures

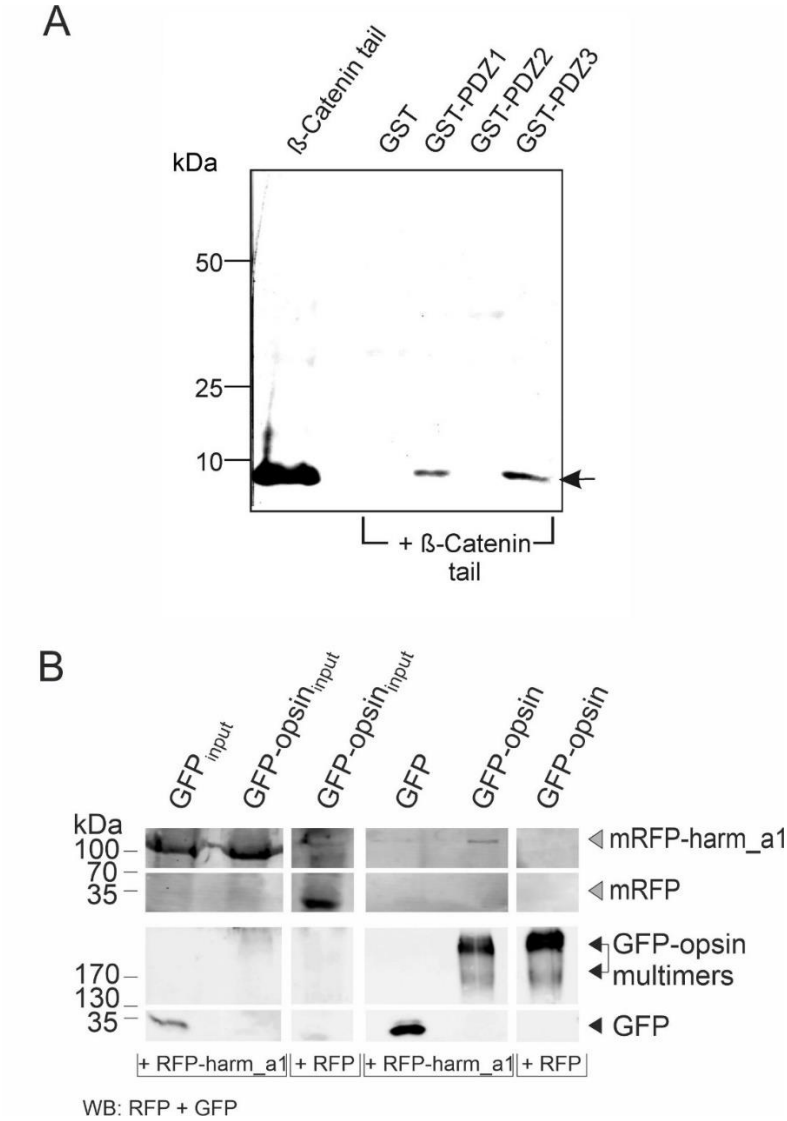

Supplemental Figure 1. Analysis of novel interaction partners of harmonin

(A) GST pull down of harmonin PDZ domains and β-catenin tail. PDZ 1 and PDZ3 of harmonin are interacting with the tail of β-catenin (β-catenin tail) GST only and harmonin PDZ2 are not interact. **(B)** GFP-Trap® demonstrate harmonin-RFP interaction with GFP-opsin. RFP-harmonin a1 was precipitated by immobilized GFP-opsin via GFP-beads, but not by GFP alone. RFP only did not interact with GFP-opsin.

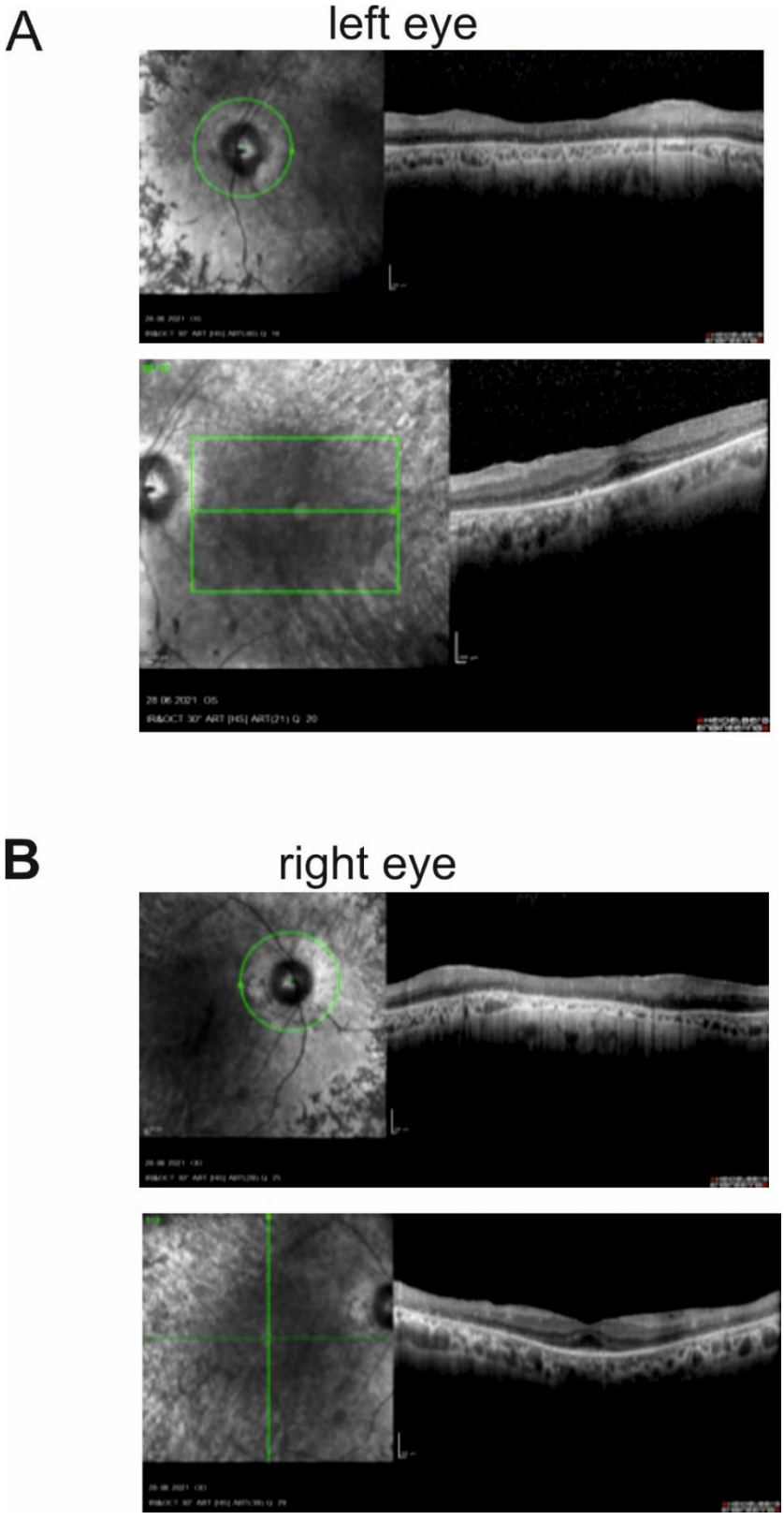

Supplemental Figure S2. OCT of USH1C patients

(A, B) Optical coherence tomography of the left (A) and right (B) eye of a 47-year old male USH1C patients with confirmed mutations in *USH1C* (c.91C>T;.p.(/R31*). c.238dupC;p.(Arg80Profs*69)) showing outer retinal atrophy with photoreceptor degeneration.

Supplemental Tables:

Supplemental Material Table S1. **Human retina donors.** AN internal donor number (#) was assigned to all donors. All donors had no documented history of retinal disease. Abbreviations: M, male, F, female, MGCs, Müller glia cells; RNs, retinal neurons; RT-PCR, reverse transcriptase polymerase chain reaction; qRT, quantitative PCR; WB, Western blot; IF, immunofluorescence microscopy; EM, electron microscopy; age in years.

Donor #	Age	Gender	*hours post mortem*	Application
198-09	56	M	30	RT-PCR
199-09	66	F	31	RT-PCR, WB, IF, EM
205-09	57	F	21	RT-PCR, RNAseq
220-09	44	F	31	RT-PCR, qRT
250-09	63	M	9 ½	RT-PCR, RNAseq
252-09	68	F	11 ½	RT-PCR, qRT, IF
263-09	56	M	27	qRT, RNAseq
269-09	73	F	29	RNAsec
121-10	58	F	21	EM
16-0928-OS	76	M	9	Bulk RNA-seq
16-0928-OD	76	M	9	Bulk RNA-seq
16-0932-OS	70	F	9	Bulk RNA-seq
16-0932-OD	70	F	9	Bulk RNA-seq
19-0013-OD	89	M	30	WB – sorted MGCs/RNs
19-0015-OS	59	F	26	WB – sorted MGCs/RNs